Integration host factor regulates colonization factors in the bee gut symbiont *Frischella perrara*

*K. Schmidt[1,3], *G. Santos-Matos[1], S. Leopold-Messer[2], Y. El-Chazli[1], O. Emery[1], T. Steiner[1], J. Piel[2] & P. Engel[1]

1 Department of Fundamental Microbiology, University of Lausanne, Lausanne, Switzerland

2 Institute of Microbiology, Eidgenössische Technische Hochschule (ETH) Zurich, Zürich, Switzerland

3 Current affiliation: Roche Diagnostics International Ltd, Rotkreuz, Switzerland

*These authors contributed equally to this work.

Correspondence:

Prof. Philipp Engel

Department of Fundamental Microbiology

University of Lausanne, CH-1015 Lausanne, Switzerland

Tel.: +41 (0)21 692 56 12

e-mail: philipp.engel@unil.ch

Abstract

Bacteria colonize specific niches in the animal gut. However, the genetic basis of these associations is often unclear. The proteobacterium *Frischella perrara* is a widely distributed gut symbiont of honey bees. It colonizes a specific niche in the hindgut and causes a characteristic melanization response. Genetic determinants required for the establishment of this association, or its relevance for the host, are unknown. Here, we independently isolated three point mutations in genes encoding the DNA-binding protein integration host factor (IHF) in *F. perrara*. These mutants abolished the production of an aryl polyene metabolite causing the yellow colony morphotype of *F. perrara*. Inoculation of microbiota-free bees with one of the mutants drastically decreased gut colonization of *F. perrara*. Using RNAseq we found that IHF affects the expression of potential colonization factors, including genes for adhesion (Type 4 pili), interbacterial competition (Type 6 secretion systems), and secondary metabolite production (colibactin and aryl polyene biosynthesis). Gene deletions of these components revealed different colonization defects depending on the presence of other bee gut bacteria. Interestingly, one of the T6SS mutants did not induce the scab phenotype anymore, despite colonizing at high levels, suggesting an unexpected role in bacteria-host interaction. IHF is conserved across many bacteria and may also regulate host colonization in other animal symbionts.

38 **Introduction**

39 The digestive tract of many animals is colonized by specialized gut symbionts that occupy distinct
40 physical niches and utilize diverse nutrients. Owing to the availability of genetic tools, gnotobiotic
41 animal models and multi-omics approaches, we can now study the genetic features that allow gut
42 symbionts to colonize various animal hosts including mammals, fishes, and insects (1-10).

43 The Western honey bee, *Apis mellifera,* is a particularly interesting model to characterize
44 colonization factors of bacterial gut symbionts, due to its agricultural importance and the
45 tractability of its gut microbiota. Honey bees harbor relatively simple yet highly specialized gut
46 microbiota composed of 8-10 bacterial genera (11, 12). The wide distribution of these
47 communities across social bees suggests long evolutionary associations with the host (13).
48 Moreover, different members of the bee microbiota colonize distinct physical niches along the gut.
49 Lactobacilli and Bifidobacteria predominate in the posterior hindgut (rectum), while
50 Gammaproteobacteria (*Frischella perrara* and *Gilliamella* species) and a Betaproteobacterium
51 (*Snodgrassella alvi*) preferentially colonize the anterior hindgut (ileum and adjacent pylorus, i.e.,
52 the transition zone between midgut and ileum) (11, 14-16). The partitioning of these bacteria into
53 distinct gut compartments suggests the existence of specific bacterial and/or host mechanisms
54 that facilitate colonization.

55 Most bacteria of the bee gut microbiota can be cultured and experiments with gnotobiotic bees
56 have been established (17-21). Moreover, genomic analyses have provided important insights
57 about the functional potential of bee gut symbionts and their adaptation to the gut environment
58 (21-29). Yet, little is known about which genes are directly involved in establishing colonization in
59 the bee gut and how these genes are regulated. The only symbiont that has been extensively
60 studied in this respect is *S. alvi.* Using transposon sequencing and transcriptome analysis, Powell
61 et al. determined genome-wide host colonization factors in *S. alvi* (7). Most genes with strong
62 fitness effects were found to belong to three major categories: extracellular interactions,
63 metabolism, and stress response. In particular, genes for attachment and biofilm formation were

64 highly beneficial for colonization, which is in agreement with the observation that this gut symbiont
65 adheres to the host epithelium of the ileum and forms a multispecies biofilm with *Gilliamella*.

66 The honey bee gut symbiont *Frischella perrara* belongs to the recently described family Orbaceae
67 within the Gammaproteobacteria (30). It is taxonomically close to the bee gut symbiont *Gilliamella*
68 and has a similar metabolism (31). However, compared to the other members of the bee gut
69 microbiota, *F. perrara* shows a rather distinctive colonization phenotype. While *S. alvi* and
70 *Gilliamella* have been reported to colonize the host epithelium of the entire ileum (32, 33), *F.*
71 *perrara* preferentially colonizes the transition zone between the midgut and the ileum, i.e., the
72 pylorus. Moreover, colonization with *F. perrara* leads to the appearance of a brown to black
73 material on the luminal side of the epithelial surface between the cuticle layer of the host tissue
74 and the adherent *F. perrara* cells (34). This so–called scab phenotype forms after 5-7 days post-
75 colonization and has so far not been reported to be triggered by any other gut symbiont than *F.*
76 *perrara*. Transcriptome analysis of the host showed that *F. perrara* elicits a specific immune
77 response which includes the upregulation of the host melanization pathway likely responsible for
78 the formation of the scab phenotype (17). *F. perrara* is highly prevalent across worker bees and
79 colonies of *A. mellifera* (34, 35), and related bacteria have also been found in *Apis cerana* (36).
80 Moreover, between 25%-80% of all worker bees of a colony harbor a visible scab phenotype in
81 the pylorus region of the gut, which has been shown to strongly correlate with a high abundance
82 of *F. perrara* (34). However, the impact of these phenotype on the host has remained elusive.

83 Genome sequencing of the type strain of *F. perrara* and comparison with other genomes of the
84 Orbaceae family revealed the presence of several genomic islands that may be involved in the
85 specific interaction of *F. perrara* with the host (37). These include a biosynthetic gene cluster for
86 the production of the genotoxic metabolite colibactin (Clb), two distinct Type VI secretion systems
87 (T6SSs) and associated effector proteins, Type I secretion systems, and fimbrial low-molecular-
88 weight protein (Flp) pili genes. However, currently no genetic tools are available for *F. perrara*
89 precluding studies about the role of these genetic factors in gut colonization or the induction of
90 the scab phenotype.

91 Here, we report the isolation of a spontaneous mutant of *F. perrara* that possesses a strong
92 colonization defect *in vivo*. Resequencing of the mutant revealed a single nonsynonymous point
93 mutation in the gene encoding the alpha subunit of the DNA-binding protein integration host factor
94 (IHF). Using a combination of gnotobiotic bee experiments, transcriptomics, and metabolite
95 analyses, we characterized the genes regulated by IHF. We then established a gene deletion
96 strategy for *F. perrara,* which allowed us to knockout some of the IHF-regulated genes and show
97 that they impact gut colonization and scab development to different extent in the presence and
98 absence of a complex community.

99 ## Results

100 **Isolation of spontaneous IHF mutants affecting growth and colony morphology of *F.***
101 ***perrara***

102 Culturing *F. perrara* type strain PEB0191 (38) on modified tryptone yeast glucose (mTYG) agar
103 resulted in the formation of yellow colonies. However, we occasionally observed the appearance
104 of larger white colonies among the yellow ones (**Figure 1A**). Restreaking white colonies on fresh
105 mTYG agar usually resulted in yellow colonies again. However, three white colonies that we
106 identified in independent experiments did not change their appearance anymore, suggesting that
107 we had isolated stable 'white' variants of *F. perrara* PEB0191 (**Figure 1B, Figure 1 - figure**
108 **supplement 1**). Genome sequencing of the white variants revealed the presence of three different
109 non-synonymous point mutations in the genes encoding the integration host factor (IHF). IHF is a
110 widely distributed DNA-binding protein consisting of the IhfA/B heterocomplex (39-41). Strikingly,
111 two point mutations were identical to each other, but occurred in the different subunits of IHF (*ihfA*
112 and *ihfB*) resulting in a proline to lysine change at amino acid position 82 and 83, respectively
113 (**Figure 1C**). The third point mutation resulted in a lysine to serine change at position 38 of IhfA
114 (**Figure 1C**). Homology modelling showed that these amino acids are located in the region
115 interacting with DNA, suggesting that the three mutations impact the DNA-binding properties of
116 IHF (**Figure 1D**, (42)). As two of the isolated mutants occurred when generating gene deletions
117 of *F. perrara,* they harbored additional genetic modifications (see Methods). Therefore, we
118 focused further characterization of IHF on the mutation Pro83Lys (hereafter *ihfA**) that occurred
119 in the wild type (wt) background of *F. perrara* PEB0191. While the *ihfA** strain consistently formed
120 larger colonies than the wt strain on mTYG agar (**Figure 1A and 1B)**, there was no significant
121 difference in growth in liquid culture (Permutation test, $p = 0.097$; **Figure 1 – figure supplement**
122 **2A**). However, light microscopy showed that cells of the mutant strain were on average slightly
123 longer than cells of the wt (Kolgomorov-Smirnov test $p<0.0001$, **Figure 1 – figure Supplement**
124 **2B and C**).

125

126 ***F. perrara* produces an aryl polyene secondary metabolite that is responsible for the yellow**
127 **colony morphotype**
128 *F. perrara* PEB0191 encodes a genomic island that is homologous to aryl polyene (APE)
129 biosynthetic gene clusters present in other Gammaproteobacteria (**Figure 2A**) (43). APEs are
130 polyunsaturated carboxylic acids conferring a yellow pigmentation to bacterial cells (44, 45). To
131 assess if *F. perrara* wt, but not the *ihfA** mutant, produces an APE, we analyzed cell extracts of
132 both strains by liquid chromatography coupled to heated electrospray ionization high-resolution
133 mass spectrometry (HPLC-HES-HRMS). The data revealed a strongly UV-Vis-absorbent ion peak
134 at *m/z* 323.1647 $[M+H]^+$, which had a suggested molecular formula of $C_{21}H_{23}O_3$ (**Figure 2B** and
135 **2C**). In the *ihfA** mutant, this ion was only present at trace amounts (**Figure 2C**). To characterize
136 the metabolite in greater detail a larger pellet of *F. perrara* wt cultures was extracted and purified
137 by several HPLC runs. Mass spectrometry- (MS) and UV-Vis-guided fractionation yielded an
138 enriched extract that was analyzed by nuclear magnetic resonance (NMR) spectroscopy. The
139 characteristic ions detected in MS-MS fragmentation experiments (**Figure 2 – figure supplement**
140 **1**), the UV-Vis spectrum with an absorption maximum at 415 nm (**Figure 2 – figure supplement**
141 **2**) in conjunction with NMR data (**Figure 2 – figure supplement 3-9, Supplementary Table 1**)
142 suggest an aryl polyene structure identical to that reported in (43, 46) (**Figure 2D**). Unfortunately,
143 it was not possible to connect the NMR substructures, because the central methines could not be
144 assigned to chemical shifts (**Figure 2D**, **Supplementary Table 1)**. Comparison of the organic
145 extracts of *F. perrara* wt and *E. coli* CFT073 provided further evidence that both produce the same
146 compound (**Figure 2 – figure supplement 10**). Combined, these results suggest that the APE
147 pathway is responsible for the yellow color of the wt colonies of *F. perrara* and is suppressed in
148 the *ihfA** mutant.

149

150 **The *ihfA** mutant of *F. perrara* has a colonization defect and does not cause the scab**
151 **phenotype**
152 As APEs have been shown to increase protection from oxidative stress and contribute to biofilm
153 formation (43, 46), we sought to test if the *ihfA** mutation impacts bee gut colonization. We mono-
154 associated microbiota-free bees with either *F. perrara* wt or *ihfA**. Colonization with the wt strain
155 resulted in a visible scab in 50% and 80% of all bees after five and ten days of colonization,
156 respectively (n=18 and n=36 for both treatments for day 5 and day 10, respectively, **Figure 3A**
157 **and 3B**). In contrast, none of the bees colonized with the *ihfA** mutant developed a visible scab
158 phenotype. To determine whether this difference was due to a general colonization defect of *ihfA**,
159 we quantified the colonization levels of *F. perrara* at day 5 and day 10 post colonization using
160 colony forming units (CFUs). While there was a trend towards lower colonization levels (fewer
161 CFUs and more bees without detectable colonization) for the *ihfA** mutant at day 5 post
162 colonization, the difference was not statistically significant (**Figure 3C**, Wilcoxon rank-sum test p-
163 value=0.076). However, at day 10 post-colonization, bees colonized with the wt strain showed
164 significantly higher CFUs than the *ihfA** mutant (**Figure 3C**, Wilcoxon rank-sum test p-
165 value<0.0001). In fact, in 50% of all bees (n = 36) the colonization levels of *ihfA** were below the
166 detection limit of 500 CFUs (colony forming units) (**Figure 3C**).
167
168 As the quantification of *F. perrara* was based on CFUs obtained for whole-gut tissue, we carried
169 out a second experiment, in which we specifically assessed the colonization levels in the pylorus
170 and the ileum region of the honey bee gut, using both CFUs and quantitative PCR (**Figure 3 -**
171 **figure supplement** 1). The results were comparable to those obtained for the whole gut: at day
172 10 post colonization, there was a significant difference in the colonization levels of the wt and
173 *ihfA** in both the pylorus and the ileum (Wilcoxon rank-sum test p-value<0.05).
174
175 To obtain a better understanding of the colonization dynamics of *F. perrara* wt and the *ihfA**
176 mutant, we conducted a third gnotobiotic bee experiment in which we inoculated microbiota-free
177 bees with one of the two strains and followed the colonization levels over 12 timepoints from day

178 0 (i.e. 4 h post inoculation) until day 22 post inoculation (**Figure 3D**). From the first time point at
179 4 h post inoculation until day 4 post inoculation, the bacterial levels were below the detection limit
180 (i.e., below 500 CFUs) in both conditions. Between day 4 and day 8 post inoculation, the
181 abundance of the wt increased rapidly to about 10^6 CFUs per gut and then steadily further to 10^7
182 CFUs per gut until the last time point. In contrast, the levels of the *ihfA** mutant remained low until
183 day 10 post colonization and reached on average no more than 10^5 CFUs per gut until the last
184 time point at day 22 post colonization. Notably, while we had used the same optical density of the
185 two strains for colonizing microbiota-free bees, dilution plating revealed that there were fewer
186 CFUs in the inocula for the wt compared to the *ihf** mutant. Despite these differences the wt
187 colonized much better than *ihfA**. In summary, these results show that *ihfA** has a strong
188 colonization defect. It has a delayed colonization dynamics as compared to the wt, does not reach
189 the same bacterial loads, and does not cause the scab phenotype, even though the bees were
190 inoculated with more viable cells of *ihfA** than the wt.
191

192 **Genes involved in symbiotic interactions are upregulated in *F. perrara* wt relative to the**
193 ***ihfA** mutant**

194 IHF may not have a direct effect on gut colonization, but rather regulate the gene expression of
195 host colonization factors. To test this, we assessed the transcriptional differences by RNA
196 sequencing (RNA-seq) between the wt and *ihfA** mutant when grown *in vitro*. We found that 358
197 out of 2,337 genes encoded in the genome of *F. perrara* were differentially expressed with a log2-
198 fold change >|2| between the two strains (Fisher's exact test with $p<0.05$ and FDR<5%). Of those,
199 237 and 121 genes were up- and down-regulated in *F. perrara* wt versus *ihfA**, respectively
200 (**Figure 4A and 4B**, **Supplementary Dataset 1**). Among the genes upregulated in the wt,
201 'Intracellular trafficking, secretion, and vesicular transport' (COG U), 'Extracellular structure' (COG
202 W), 'Lipid transport and metabolism' (COG I), 'Mobilome: prophages and transposases' (COG X),
203 and 'Secondary metabolites biosynthesis, transport and catabolism' (COG Q) were significantly
204 enriched (Fisher's exact test, BH-adjusted p-value < 0.01; see **Supplementary Dataset 2**).

205 Genes belonging to these three categories include different subunits and effectors of the two
206 T6SSs of *F. perrara*, the Clb biosynthesis gene cluster, various components of the Flp pili, and a
207 RTX (repeats in toxin) toxin belonging to the Type I secretion system family (**Supplementary**
208 **Dataset 1**). Also, the genes of the APE biosynthesis gene cluster were among the upregulated
209 genes, which is in line with the production of the corresponding metabolites in the wt but not in
210 the mutant strain (**Figure 2**). Interestingly, a relatively large proportion of the upregulated genes
211 encoded hypothetical or poorly characterized proteins. In fact, genes without COG annotation
212 were also enriched relative to the entire genome of *F. perrara* (Fisher's exact test, BH-adjusted
213 p-value < 0.01; see Supplementary **Dataset 2**). Many of the upregulated genes were organized
214 in genomic islands, with the largest one including the biosynthesis gene cluster of Clb and many
215 hypothetical protein-encoding genes (**Figure 4C**). T6SS and Clb biosynthesis genes were among
216 the genes with the highest fold changes relative to *ihfA** mutant (**Figure 4B**, 28 of 32 genes with
217 log2-fold change >6). Moreover, 64% of the upregulated genes (152/237) belonged to the *F.*
218 *perrara*-specific gene content as based on our previously published genome comparison of *F.*
219 *perrara* PEB0191 with four other strains of the family Orbaceae (three of the genus *Gilliamella*
220 and one of the genus *Orbus*, **Supplementary Dataset 1)** (37).

221 Among the 121 down-regulated genes, only COG category O ('Posttranslational modification,
222 protein turnover, chaperones') was statistically enriched (Fisher's exact test, BH-adjusted p-value
223 < 0.01, see **Supplementary Dataset 2**). Moreover, only a small fraction (12%) belonged to the
224 "*F. perrara*-specific genes", and fewer genes were organized into genomic islands. A more
225 detailed inspection of the annotation revealed that a large number of the down-regulated genes
226 were involved in transport and metabolism (40 genes), transcriptional regulation (10 genes), and
227 protein folding (8 genes), highlighting clear differences in the functional roles of the up- and down-
228 regulated genes. The two genes with the highest fold change (log2-fold change <-5) both encoded
229 transcriptional regulators. One of them, *dksA* (Fpe_01158), is located upstream of the *mrsA*/*mrsB*
230 antioxidant system (Fpe_01159 to Fpe_01162), which was also among the down-regulated
231 genes. The other one is part of the two-component regulator system *basS*/*basR* (Fpe_02097 and

232 Fpe_02098), which has been reported to act as an iron- and zinc-sensing transcriptional repressor
233 and activator in *E. coli* (47, 48). Taken together, these results show that many accessory genes
234 known to be involved in symbiotic interactions (colibactin, Flp pili, T6SS) are upregulated in *F.*
235 *perrara* wt as opposed to *ihfA**, providing a list of candidate genes responsible for the colonization
236 defect of the *ihfA** mutant.

237

238 **T6SS, pili, APE biosynthesis and Clb biosynthesis genes are expressed during bee gut**
239 **colonization**

240 To test if the genes upregulated *in vitro* in the wt relative to *ihfA** were expressed *in vivo*, we
241 determined the transcriptome of *F. perrara* wt at day 5 and day 10 post colonization. A total of
242 260 (149 up and 111 down) and 298 (162 up and 136 down) genes were differentially expressed
243 at day 5 and day 10 post colonization relative to growth *in vitro* (log2-fold change >|2|, quasi-
244 likelihood F-test with $p<0.05$ and FDR<5%, **Supplementary Dataset 3**). There was a
245 considerable overlap of the differentially regulated genes between the two time points (115 and
246 80 shared up- and down-regulated genes, respectively). At both time points, the COG category
247 'Carbohydrate transport and metabolism' (COG G) was significantly enriched among the genes
248 upregulated *in vivo* relative to the entire genome (**Supplementary Dataset 4**). In addition, at time
249 point day 10, also the COG category (P) 'Inorganic ion transport and metabolism' was enriched
250 (P adj < 0.01, Fisher's exact test, **Supplementary Dataset 4**). Genes belonging to these two
251 categories encoded transporters for different sugars (Phosphotransferase systems), iron, and
252 transferrin (**Figure 5 – figure supplement 1, Supplementary Dataset 3**). In addition, a catalase
253 gene and several genes for the biosynthesis of the amino acid tryptophan were upregulated at
254 both time points. However, only 14 and 19 genes of those upregulated *in vitro* in the wt relative to
255 the *ihfA** mutant (see **Figure 5**), were also upregulated *in vivo* at day 5 and day 10 post-
256 colonization, respectively (**Supplementary Dataset 3**). This was expected, because the *in vitro*
257 RNAseq analysis had shown that these genes are already expressed in the wt when grown on
258 mTYG agar, which we used as a reference condition for the *in vivo* analysis. Indeed, when

259 comparing count-normalized gene expression (as measured by Transcripts per million (TPM))
260 across the different conditions, we found that most of the T6SS machinery, APE biosynthesis,
261 pilus, and iron uptake genes were expressed at both time points *in vivo*, and to similar levels as
262 *in vitro* (**Figure 5, Figure 5 – figure supplement 2**). Only the Clb genomic island and some of
263 the VgrG-like T6SS effector genes had clearly lower TPM values *in vivo* than *in vitro*, yet higher
264 than in *ihfA* in vitro* (**Figure 5C and 5F**). These results suggest that most of the genes upregulated
265 *in vitro* in the wt relative to *ihfA** are also expressed at high level by the wt *in vivo*.
266
267
268 **Gene deletion of IhfA-regulated genes result in impaired gut colonization and/or abolish**
269 **scab development**
270 To test the direct impact of IhfA-regulated genes on host colonization and/or scab development
271 we established a gene deletion strategy for *F. perrara* based on a two-step homologous
272 recombination procedure (see methods and **Figure 6 – figure supplement 1**). This allowed us
273 to create six different non-polar in-frame gene deletion mutants of potential colonization factors
274 regulated by IHF (Supplementary Table S2). We deleted an essential gene of the colibactin
275 biosynthesis pathway (Δ*clbB*), both *hcp* genes of the two T6SSs, either separately or as double
276 mutant (Δ*hcp1,* Δ*hcp2,* and Δ*hcp1*/Δ*hcp2*), the gene encoding the major Flp pili subunit (Δ*pilE*),
277 and the entire APE biosynthesis gene cluster (Δ*apeA-R*). Deletion mutants were confirmed by
278 genome re-sequencing. The Δ*apeA-R* mutant was the only strain not forming yellow colonies
279 anymore (**Figure 1 – figure supplement 1**), which is consistent with the idea that the aryl polyene
280 pathway is responsible for the yellow color. We measured the growth of the gene deletion mutants
281 *in vitro,* which was similar to the wt and *ihfA** strains **(Figure 6 – figure supplement 2)**.
282 Additionally, no significant differences were observed in cell length **(Figure 6 – figure**
283 **supplement 3)**. Moreover, we corresponded OD_{600} to CFU counts and found that both the
284 Δ*hcp1*/Δ*hcp2* and Δ*pilE* strains had lower counts than the wt strain **(Figure 6 – figure supplement**
285 **4)**. To compare the six gene deletion strains to *F. perrara* wt and the *ihfA** mutant in terms of gut

286 colonization and induction of the scab phenotype, each strain was inoculated into microbiota-free
287 bees and CFUs assessed in the pylorus/ileum region ten days post inoculation. As expected, the
288 wt successfully colonized the pylorus/ileum region of all analyzed gnotobiotic bees (median =
289 $9.56*10^6 \pm 5.06*10^6$ CFUs per gut; n=18 bees, two independent experiments) and induced the scab
290 phenotype in 16 of 18 bees (**Figure 6A and Figure 6 – figure supplement 5**). In contrast, the
291 *ihfA** colonized poorly compared to the wt (median=$1.46*10^4 \pm 3.19*10^5$ CFUs per gut, n= 20 bees,
292 Wilcoxon rank-sum test $P<0.001$), and not a single bee developed the scab phenotype. Of the six
293 tested gene deletion mutants, only the mutant of T6SS-1 (Δ*hcp1*) reached wt colonization levels
294 and also induced the scab phenotype in most of the bees (15 out of 20). The other five mutants
295 all exhibited lower colonization levels than the wt strain. However, the severity of the colonization
296 defect varied between the mutants, and while some of the mutants still caused the scab
297 phenotype, others did not. For example, the Clb biosynthesis gene cluster mutant Δ*clbB* induced
298 the scab phenotype in all but one bee, despite the fact that the colonization levels were about
299 two-fold lower than for the wt (median=$4.24*10^6 \pm 2.87*10^6$ CFUs per gut). The gene deletion
300 mutant of the T6SS-2 (Δ*hcp2*) and the double mutant of both T6SSs (Δ*hcp1*/Δ*hcp2*) reached
301 similar colonization levels as the Δ*clbB* mutant. Yet, none of the bees colonized with these two
302 mutants developed the scab phenotype, not even those that had very high bacterial counts
303 (**Figure 6A**). The deletion mutant of the APE biosynthesis pathway (Δ*apeA-R*) showed again a
304 different colonization phenotype: for some bees no colonization was detected, while others
305 showed similar colonization levels as the wt of *F. perrara*. However, in contrast to the Δ*hcp2* and
306 the Δ*hcp1*/Δ*hcp2* mutants, the Δ*apeA-R* mutant still induced the scab phenotype, but only in the
307 bees that had high bacterial loads. Finally, the Δ*pilE* mutant had the strongest impact on
308 colonization. Only five out of 20 bees had detectable levels of *F. perrara* in the gut (limit of
309 detection: 75 CFUs per gut) and none of the bees developed the scab phenotype. Electron
310 microscopy imaging revealed this strain did not have pili, confirming the Δ*pilE* mutation affects the
311 formation of these structures **(Figure 6 – figure supplement 3C).**

312 The Δ*clbB,* Δ*hcp2* and Δ*hcp1*/Δ*hcp2* mutants all reached similar colonization levels, yet only
313 colonization with Δ*clbB* led to the development of the scab phenotype. These differences in scab
314 formation could be due to an altered colonization pattern of the Δ*hcp2* and Δ*hcp1*/Δ*hcp2* mutants.
315 To address this hypothesis, we visualized how the gene-deletion mutants are distributed in the
316 pylorus (**Figure 6B, Figure 6 – figure supplements 6 and 7**). We obtained cross-sections of the
317 pylorus of bees associated with these mutants, stained them with DAPI and a *F. perrara*-specific
318 FISH probe and imaged these sections using confocal microscopy. As previously reported (34),
319 *F. perrara* wt was found to colonize the pylorus region, forming a dense biofilm in close proximity
320 to the host and occupying the crypts. A similar colonization pattern was observed for Δ*hcp1*,
321 Δ*hcp2*, Δ*hcp1*/Δ*hcp2,* Δ*clbB* and Δ*apeA-R.* In contrast, for the *ihfA** and Δ*pilE* mutants, we did not
322 identify any bacteria in the analyzed gut sections which is in agreement with the low colonization
323 levels of these mutants detected by CFU plating. Dark spots corresponding to scab material were
324 found along the cuticular lining colonized by bacteria for the Δ*clbB,* Δ*hcp1* and Δ*apeA-R,* but not
325 for the Δ*hcp2* and Δ*hcp1*/Δ*hcp2* mutants, which matches the visual inspections of the dissected
326 guts for the presence/absence of the scab phenotype across the different strains (**Figure 6B**).
327 Based on these results, we conclude that the inability of the Δ*hcp2* and Δ*hcp1*/Δ*hcp2* mutants to
328 trigger the scab phenotype cannot be explained by an altered localization in the gut. Overall, these
329 results confirm that IHF regulates various host colonization factors that when deleted cause
330 distinctive colonization defects.
331

332 ***F. perrara* T6SS-2 and the APE biosynthesis pathway regulate gut colonization in complex**
333 **bacterial communities**

334 In natural conditions, *F. perrara* shares its niche with other symbionts of the bee gut. As several
335 factors regulated by IHF are known for their role in microbial interactions (49, 50), we also wanted
336 to test the impact of the six gene-deletion mutants on the ability of *F. perrara* to colonize the bee
337 gut in the presence of other community members. We compared gut colonization levels of the
338 gene deletion mutants, *ihfA*,* and the wt in the presence and absence of a synthetic community

339 (BeeComm_002) composed of 13 strains representing major core microbiota members of the
340 honey bee gut microbiota (detailed information in **Supplementary Table 4**). For five of the eight
341 tested strains we did not detect a significant effect of the BeeComm_002 on the colonization levels
342 (**Figure 7, Figure 7 – figure supplement 1**). This included *F. perrara* wt, which successfully
343 colonized the gut independently of the presence of the BeeComm_002 (Wilcoxon rank-sum test
344 P=0.899, two independent experiments), the *ihfA** (Wilcoxon rank-sum test P=0.638) and the pili
345 mutant Δ*pilE* (Wilcoxon rank-sum test P=0.217), which both already exhibited a strong
346 colonization defect in mono-colonization, and the colibactin gene cluster mutant Δ*clbB* (Δ*clbB:*
347 Wilcoxon rank-sum test P=0.127) and the T6SS-1 mutant Δ*hcp1* (Wilcoxon rank-sum test
348 P=0.068), which both colonized at equal levels in both conditions (**Figure 7**). For the other three
349 mutants we observed a significant reduction in colonization levels in the presence of the
350 BeeComm_002. The colonization levels of T6SS-2 mutant Δ*hcp2* decreased seven-fold (median
351 mono-association: $3.86*10^7 \pm 4.16*10^7$, median BeeComm_002: $5.10*10^6 \pm 1.77*10^7$, Wilcoxon
352 rank-sum test P=0.002) whereas both the T6SS double mutant Δ*hcp1/hcp2* (Wilcoxon rank-sum
353 test P=0.029) and the APE biosynthesis mutant Δ*apeA-R* (Wilcoxon rank-sum test P=0.004) failed
354 to colonize most bees tested **(Figure 7 and Figure 7 -figure supplement 1B)**. These results
355 demonstrate that the T6SS-2 and the APE biosynthesis pathway play a role in regulating *F.perrara*
356 colonization in the presence of other symbionts, possibly regulating the interaction with these
357 bacterial partners.
358
359

360 **Discussion**

361 In this study, we identified genetic factors that allow the gut symbiont *F. perrara* to colonize its
362 specific niche in the pylorus of the honey bee gut and to induce the scab phenotype. Our results
363 advance the understanding of the genetic factors that facilitate symbionts to colonize niches in
364 the animal gut. Specifically, we find that the DNA-binding protein IhfA plays an important role in
365 gut colonization. IhfA is a histone-like, nucleoid-associated protein (NAP) that forms a heterodimer
366 together with IhfB. IHF binds to and bends DNA in a sequence specific manner (40-42, 51),
367 thereby facilitating the recombination of mobile DNA elements (40, 41) and influencing gene
368 expression. We identified three different mutations in IHF, all located in the region of the protein
369 interacting with the DNA. All three IHF mutants formed larger colonies than the wt strain on mTYG
370 agar. Together, this suggests that the identified mutations change the DNA-binding properties of
371 IHF resulting in broad transcriptional changes in *F. perrara* that provide a growth advantage *in*
372 *vitro* relative to the wt strain.

373 *F. perrara* colonizes the epithelial surface of the pylorus, where it adheres to the cuticular lining
374 and forms a thick biofilm-like layer (34). IHF has been shown to bind to extracellular DNA, which
375 in the case of the human pathogen *Haemophilus influenzae* increases biofilm stability (52).
376 Therefore, it is possible that IHF has a direct impact on gut colonization of *F. perrara* by stabilizing
377 the biofilm formed on the host epithelium. However, based on our gene expression data and the
378 results of the gene deletion experiments, it seems more likely that IHF influences gut colonization
379 by regulating downstream genes involved in host interaction. Several of the genes regulated by
380 IHF are known to play important roles in the adhesion to surfaces or the formation of biofilms. For
381 example, pili are key factors for adhesion across many bacteria (53-56) and have already been
382 shown in the case of the bee gut symbiont *S. alvi* to be beneficial for gut colonization and biofilm
383 formation (7). In agreement with these previous results, several of the deletion mutants of IHF-
384 regulated genes showed colonization defects in our gnotobiotic bee experiments corroborating
385 that IHF impacts gut colonization through its effect on gene expression rather than through a direct
386 role in biofilm formation.

387 The pili mutant (Δ*pilE*) had the strongest colonization defect of the tested gene deletion strains,
388 likely because pili mediate the adhesion to the host epithelium, and therefore allow *F. perrara* to
389 persist and replicate in the pylorus/ileum region of the honey bee gut. The deletion mutant of the
390 APE biosynthesis pathway (Δ*apeA-R*) also showed a clear colonization defect. However, while
391 some of the bees inoculated with this mutant had no detectable levels of *F. perrara* in the gut,
392 others reached similar levels as bees colonized with the wt strain and also developed the scab
393 phenotype. Aryl polyenes can protect bacteria from reactive oxygen species (46, 57) which are
394 produced by insects as part of the host immune response in the midgut (58, 59). Our time course
395 experiment revealed that in the first few days of colonization the bacterial numbers of *F. perrara*
396 in the gut are much lower than in the initial inoculum (**Figure 2**) suggesting that the bacteria
397 experience a significant population bottleneck at the beginning of the colonization process. It is
398 possible that the Δ*apeA-R* mutant is impaired in its ability to resist reactive oxygen species (or
399 other physicochemical stressors) when passing through the anterior sections of the honey bee
400 gut and therefore reaches its niche in the pylorus in only a fraction of the inoculated bees. These
401 stressors may be even more active in the presence of a complex community, which could explain
402 the even lower colonization success of Δ*apeA-R* in the presence of the BeeComm_002. However,
403 APEs have also been implicated in other functions such as biofilm formation (57). Therefore,
404 future studies will be needed to elucidate how the APE biosynthetic pathway of *F. perrara* impacts
405 honey bee gut colonization. Given the widespread occurrence of these biosynthetic genes
406 throughout different bacteria, this might help to understand their role in host colonization in a much
407 wider context (43).

408 A somewhat unexpected result of our mutant analysis was that the deletion of one of the genes
409 encoding an essential NRPS/PKS enzyme (ClbB) of the Clb biosynthetic gene cluster did not
410 affect scab development and had only a weak impact on gut colonization (2-fold lower levels than
411 wt). Studies on *E. coli* have shown that the Clb biosynthesis pathway induces DNA damage in
412 eukaryotic cells (60) and contributes to tumorigenesis in the mammalian gut (61, 62). We have
413 previously shown that *F. perrara* also induces DNA damage in eukaryotic cells and that this is

414 dependent on a functional Clb biosynthesis pathway (37). Therefore, we had speculated that the
415 genotoxic activity of colibactin may trigger the local melanization response and the development
416 of the scab phenotype upon colonization with *F. perrara* (17, 34). However, the results presented
417 here show that colibactin is not causing the scab phenotype. Therefore, other characteristics of
418 *F. perrara* must explain why this bacterium causes the scab phenotype.

419 Usually, bees that have $<10^6$ bacteria in the gut do not develop visible scab at day 10 post
420 colonization (**Figure 3 and Figure 7**), which suggests that a certain number of bacteria is needed
421 to elicit this characteristic host response. On the contrary, not all bees with high levels of
422 colonization developed a scab phenotype indicating that high loads are necessary but not
423 sufficient to trigger the development of a visible scab phenotype. Specifically, the *Δhcp2* mutant
424 of T6SS-2 and the *Δhcp1*/*Δhcp2* double mutant of T6SS-1 and T6SS-2 both reached relatively
425 high colonization levels, yet not a single bee developed the scab phenotype. T6SS are usually
426 involved in interbacterial warfare by injecting toxins into neighboring bacterial cells (63-65).
427 However, there is an increasing number of studies showing that certain T6SS effectors can also
428 target eukaryotic cells and modify diverse eukaryotic processes, including adhesion modification,
429 stimulating internalization, cytoskeletal rearrangements and evasion of host innate immune
430 responses (66). While *F. perrara* is not the only bee gut symbiont harboring T6SS, the effector
431 protein repertoires differ tremendously between different species and even strains of the same
432 species (67). Thus, it is possible that some of the effector proteins of *F. perrara* may target the
433 host rather than other bacteria eliciting the melanization response and scab phenotype in the bee
434 gut. Additionally, both the *Δhcp2* and the *Δhcp* double mutant had increased colonization defects
435 in the presence of the BeeComm_002. This raises the hypothesis that the T6SS-2 may be
436 important for *F.perrara* to interact with other gut symbionts, namely bacteria of the genera
437 *Snodgrassella* and *Gilliamella* that also colonize the pylorus. It is important to mention that our
438 experimental design favored *F. perrara* over the individual members of the BeeComm_002 as, in
439 the inoculum fed to the bees, *F. perrara* was 13 times more abundant than any member of the
440 defined community. It is likely that a stronger colonization defect would be observed if the

441 proportions of *F. perrara* to other community members were more even. In any case, the presence
442 of the BeeComm_002 led to a reduction of the number of bees colonized by most *F. perrara*
443 strains, but not for the wt **(Figure 7 – figure supplement 1B)**. This is particularly interesting in
444 the case of the *Δhcp1* and *ΔclbB* mutants, suggesting a possible role for these genes in the
445 presence of other symbionts.

446 We did not carry out a genome-wide screen for host colonization factors, and only generated
447 deletion mutants of a few of the IHF-regulated genes. Thus, there are probably many other factors
448 that also contribute to gut colonization. For example, our *in vivo* RNA-seq experiment indicated
449 that metabolic genes involved in tryptophan biosynthesis, sugar transport, and iron uptake are
450 upregulated during gut colonization. This is in line with the TnSeq screen performed in *S. alvi,*
451 which revealed that genes of essential amino acid biosynthesis pathways and iron uptake are
452 important colonization factors of the honey bee gut (68). It is however remarkable that *F. perrara*
453 only upregulates the tryptophan biosynthesis pathway, which suggest a specific demand for the
454 production of this specific amino acid during gut colonization.

455 While our study revealed that IHF is important for regulating host colonization factors in the honey
456 bee gut, it remains to be elucidated whether IHF is a direct regulator of the identified genes. In
457 *Vibrio fluvialis*, IHF binding sites were identified upstream of several T6SS gene clusters,
458 indicating that direct transcriptional regulation of similar genes by IHF exists in other bacteria (69).
459 Alternatively, IHF may act upstream of another regulator that controls the expression of the
460 identified genes. In the plant pathogen *Dickeya zeae,* IHF was suggested to positively regulate
461 different virulence factors through binding to the promoter region of a diguanylate cyclase gene,
462 increasing the production of the secondary messenger c-di-GMP (70). In *F. perrara,* we found that
463 the transcriptional regulators BasR and DksA were substantially downregulated in the wt versus
464 the *ihfA** mutant. Hence, it is possible that at least some of the differentially regulated genes may
465 not be under the direct control of IHF but regulated via BasR or DskA.

466 In conclusion, we identified important gut colonization factors of the bee gut symbiont *F. perrara*
467 and show that they are regulated by IHF. The wide occurrence of these genes in host-associated

468 bacteria suggests similar roles in other environments and calls for a more detailed functional
469 characterization. Our approach to create clean gene deletion mutants expands the available
470 genetic toolbox for bee symbionts (33) and will help to dissect the molecular mechanisms of the
471 identified gut colonization factors in this animal model.

472

473 ## Material and methods

474 ### Bacterial cultivation

475 *F. perrara* strains were cultivated on modified tryptone yeast extract glucose (mTYG) medium
476 (0.2% Bacto tryptone, 0.1% Bacto yeast extract, 2.2 mM D-glucose, 3.2 mM L-cysteine, 2.9 mM
477 cellobiose, 5.8 mM vitamin K, 1.4 µM $FeSO_4$, 72.1 µM $CaCl_2$, 0.08 mM MgSO4, 4.8 mM NaHCO3,
478 1.36 mM NaCl, 1.8 µM Hematine in 0.2 mM Histidine, 1.25% Agar adjusted to pH 7.2 with
479 potassium phosphate buffer), Columbia Blood Agar (CBA) containing 5% defibrinated sheep
480 blood (Oxoid)) or Brain Heart Infusion broth (BHI) and incubated in anaerobic conditions at 34-
481 35 °C (8% H_2, 20% N_2, 78% CO_2 in a Vinyl Anaerobic Chamber, Coy Lab). Fresh bacterial cultures
482 were used for each experiment. To this end, pre-cultures streaked out from glycerol stocks were
483 grown for 48 hours and re-inoculated onto fresh plates for 16-24 hours of growth. For liquid
484 cultures, pre-cultures streaked out from glycerol stocks were grown on TYG or BHIA plates for 48
485 hours and then inoculated into fresh liquid TYG or BHI. Cultures were incubated at 34-35 °C in a
486 ThermoMixer C (Eppendorf) at 800 rpm for 16-24 hours of growth. Strains of *F. perrara* used in
487 this study are listed in **Supplementary Table S2**.

488

489 ### Rearing and experimental colonization of honey bees

490 Microbiota-depleted bees were generated as described by (18). For experimental mono-
491 colonization, bees were starved for 1-3 hours by removal of the sugar water solution. Then, bees
492 were cooled down to 4 °C in a refrigerator or on ice to transfer them (head side first) into 1.5 ml
493 microfuge tubes with a hole at the bottom. Tubes with bees were kept at room temperature. For
494 inoculation, each bee was fed 5 µl of *F. perrara* resuspended in sugar water:PBS (1:1 v/v) through
495 the hole at the bottom of the microcentrifuge tube. The bacterial inocula were adjusted to an OD_{600}
496 of 0.01 or 0.1 depending on the experiment. Colonized bees were kept at 30 °C with 70% humidity
497 while having access to sugar water and sterilized bee pollen *ad libitum* until sampling.

498

499 **Tissue dissection and bacterial quantification from colonized honey bees**

500 Bees were anesthetized by exposure to CO_2. The whole gut or desired gut tissue, e.g., pylorus or
501 ileum was dissected using a scalpel. Malpighian tubules were removed from the gut tissue and
502 the presence of a scab was documented using a dissection stereomicroscope (Leica) as
503 described in (14, 17). The tissues were placed into 2 ml screw-cap tubes containing glass beads
504 (0.75-1 mm diameter, Roth) and 500-1000 µl PBS depending on the experiment. Homogenization
505 of the sample was done by bead beating (FastPrep-24 5g MP Biomedicals) for 40 seconds at a
506 speed of 7.5 m/s. Serial dilutions (1:10) were performed for each homogenate and plated onto
507 mTYG or BHI agar. Single colonies were counted to determine the total number of bacteria per
508 gut tissue by multiplying with the dilution factor.

509

510 **RNA sequencing of bacterial *in vitro* cultures**

511 Fresh *F. perrara* cultures were prepared on mTYG plates, harvested, and directly transferred into
512 a tube containing TRI reagent (Sigma-Aldrich, Merck) and silica beads (0.1 mm diameter, Roth).
513 Samples were immediately snap frozen in liquid nitrogen and stored at -80 °C until RNA
514 extraction. RNA was extracted using a modified TRI reagent protocol. Samples were
515 homogenized by bead beating with a FastPrep instrument with CoolPrep adapter (FastPrep-24
516 5G, cooled with dry ice) for two cycles of 45 seconds at speed of 6 m/s, including a 30 seconds
517 break between each cycle. Samples were kept at room temperature for 5 min, subsequently
518 extracted using chloroform and RNA was precipitated using isopropanol overnight at -20 °C.
519 Precipitated RNA was dissolved in RNase-free water (Gibco) and incubated with DNase (NEB) to
520 degrade remaining DNA. RNA samples were cleaned up using NucleoSpin RNA clean up kit
521 (Machery-Nagel) according to manufacturer's protocol, eluted in RNAse-free water and stored at
522 -80 °C until further use. RNA quality was assessed using Nanodrop, Qubit RNA HS kit
523 (ThermoFisher Scientific) and Bioanalyzer instrument (Agilent). High quality RNA samples were
524 sent to Lausanne Genomic Technology Facility (GTF, University of Lausanne) for RNA
525 sequencing. Samples were depleted of 16S rRNA using RiboZero reagent (Illumina) and Truseq

526 stranded-RNA Zero libraries were generated (Illumina) before sequencing on an Illumina
527 HiSeq2500 generating single-end 100 bp reads.

528

529 **RNA sequencing of bacteria during honey bee gut colonization**

530 Microbiota-depleted bees were colonized with freshly grown *F. perrara*. A fraction of the inoculum
531 was directly transferred into 2 ml tube containing TRI reagent (Sigma-Aldrich, Merck) and silica
532 beads (0.1 mm diameter, Roth). These samples were immediately snap-frozen in liquid nitrogen
533 and stored at -80 °C until RNA extraction, which was carried out in the same way as described in
534 the previous section. For the *in vivo* RNA samples, bees were colonized with *F. perrara* as
535 described above and sampled at day 5 and day 10 post inoculation. Guts were removed from
536 anesthetized bees, the pylorus and first part of the ileum was dissected, and the presence of the
537 scab was recorded. For each sample, 10 pylorus and ileum sections from bees coming from the
538 same cage were pooled in a 2 ml screw cap tube containing 750 µl of TRI reagent (Sigma-Aldrich,
539 Merck), glass beads (0.75-1 mm diameter, Roth), and silica beads (0.1 mm diameter, Roth).
540 Immediately after collection, samples were snap frozen in liquid nitrogen and stored at -80 °C until
541 RNA extraction. RNA was extracted as described in the previous section. At each time point, four
542 biological replicate samples were used for RNA sequencing, i.e., bees for one sample came from
543 independent cages of gnotobiotic bees. The GTF at the University of Lausanne generated the
544 libraries for the sequencing of the *in vivo* RNA samples. Poly-A depletion was performed in order
545 to enrich for bacterial mRNA and Ribo-zero rRNA depletion was performed in order to remove
546 prokaryotic and eukaryotic rRNAs. Then TruSeq stranded mRNA libraries (Illumina) were
547 generated. The eight libraries were sequenced on an Illumina HiSeq 2500 to obtain single-end
548 125 bp reads. Libraries of the *in vitro* RNA samples were generated as described before. The four
549 libraries corresponding to the *F. perrara* inocula used for colonizing the bees of the four replicates
550 were sequenced on an Illumina MiniSeq at the Department of Fundamental Microbiology (125 bp
551 single-end reads). Two *in vivo* samples (sample identifier D10_3M and D5_1M) sequenced on

552 the HiSeq 2500 at the GTF were included in the MiniSeq run which confirmed that the two runs
553 gave comparable results.

554

555 **Differential gene expression and gene enrichment analysis**

556 Raw FASTQ files provided by the GTF containing all reads and corresponding tags indicating
557 whether they were accepted or filtered out according to the CASAVA 1.82 pipeline (Illumina). Only
558 reads tagged as accepted were kept for further analysis. FASTQC
559 (http://www.bioinformatics.babraham.ac.uk/projects/fastqc/) was used to control the quality of the
560 data, followed by Trimmomatic (Trimmomatic-0.35) to trim adapters. Filtered and trimmed reads
561 were mapped onto the *F. perrara* genome using Bowtie (bowtie2-2.3.2*)*. Mapped reads were
562 quantified using HTseq (Version 0.7.2). Differential gene expression analysis was done with the
563 Bioconductor package EdgeR (71) using R scripts. For the in vitro RNAseq analysis, negative
564 binomial models were fitted to the data and quantile-adjusted conditional maximum likelihood
565 (qCML) common and tagwise dispersion were estimated. The conditional distribution for the sum
566 of counts in a group was used to calculate the significantly differentially expressed genes using
567 an Exact test with a false discovery rate <5%. Only genes detected in all samples with at least 1
568 count per million were used for the analysis. For the in vivo RNAseq analysis, we followed the
569 recommendations specified in the EdgeR user guide for generalized linear models. In short, read
570 counts were normalized by trimmed mean of M-values (72) producing scaling factors used by
571 EdgeR to determine effective library sizes. Then, negative binomial generalized linear models
572 were fitted for each condition and quasi-likelihood F-tests for each defined contrast (i.e., pairwise
573 comparison between conditions) was used to assess the significance of differentially expressed
574 genes. As for the in vitro RNAseq analysis, only genes with mapped reads with at least 1 count
575 per million in all replicates and conditions were used for the analysis. Genes were considered as
576 differentially expressed upon fulfilling the following criteria: (i) log2 fold change ≥ 2 (ii) a p-value
577 of <0.05 and (iii) a false discovery rate <5%. Transcripts per million (TPM) were calculated as
578 follows (73):

579 $$TPM\ of\ a\ gene = \frac{number\ of\ mapped\ reads * read\ length * 10^6}{total\ number\ of\ transcripts\ sampled * gene\ length\ in\ bp}$$

580 Coverage plots in **Figure 2A** and **Figure 4C** were generated with bam2wig.pl contained in the
581 Bio-ToolBox-1.68 (https://github.com/tjparnell/biotoolbox) and visualized with the Integrated
582 Genome Browser (74). Scripts for analyzing the RNAseq data can be found under the following
583 Switchdrive link: https://drive.switch.ch/index.php/s/kCNTp4g7n60ffMi.

584

585 **DNA extraction of dissected gut tissue homogenates**

586 DNA/RNA extraction was performed using an adapted hot phenol protocol from (18) consisting of
587 sample thawing on ice, homogenization by bead beating at 7.5 m/s for 40 seconds (FastPrep-24
588 5g MP Biomedicals), two phenol extractions, and an ethanol precipitation overnight at -80 °C.
589 DNA/RNA mixture was pelleted and eluted in RNase free water (Gibco). Samples were treated
590 with RNaseA and DNA was purified using a Gel and PCR purification kit (Machery-Nagel). For
591 those samples displayed in Figure 7 and Figure 7 – figure supplement 1, samples were
592 homogenized with 165µL of a solution containing GI lysis buffer, Quiagen™, and lysozyme (10:1
593 concentration) zirconia beads (0.1 mm dia. Zirconia/Silica beads; Carl Roth) and glass beads in
594 a Fast- Prep24 5G homogenizer (MP Biomedicals) at 6 m/s for 45 s. After homogenization,
595 samples were incubated at 37°C for thirty minutes. Then, 30µL of Proteinase K were added and
596 samples were incubated at 56°C for one hour. The purification of nucleic acids was performed
597 using CleanNGS magnetic beads (CNGS-0005) and the Opentron OT-2 pipetting robot. Purified
598 DNA extracts were stored at -20°C until further use.

599

600 **Bacterial quantification by qPCR**

601 Bacterial absolute abundances were determined using quantitative PCR (qPCR) assays targeting
602 the 16S rRNA gene of *F. perrara*. Normalization was based on the number of host actin gene
603 copies as described in (18, 75). Primer sequences and other primer characteristics are given in

604 **Supplementary Table S3**. qPCR was conducted on a StepOne Plus instrument (Applied
605 Biosystems) with the following run method: a holding stage consisting of 2 min at 50 °C followed
606 by 2 min at 95 °C, 40 cycles of 15 sec at 95 °C, and 1 min at 65 °C. A melting curve was generated
607 after each run (15 sec at 95 °C, 20 sec at 60 °C and increments of 0.3 °C until reaching 95 °C for
608 15 sec) and used to assess specificity of PCR products. qPCR reactions were performed in 10
609 µL reactions in triplicates in 96-well plates, and each reaction consisted of 1 µL of DNA, 0.2 µM
610 of forward and reverse primer and 1x SYBR green "Select" master mix (Applied Biosystems). The
611 qPCR reactions for the data corresponding to Figure 7 and Figure 7 – figure supplement 1 were
612 carried out in 384-well plates on a QuantStudio™ 5 (Applied Biosystems). The thermal cycling
613 conditions were as follows: denaturation stage at 50°C for 2 min followed by 95°C for 2 min, 40
614 amplification cycles at 95°C for 15 s, and 60°C for 1 min. Each reaction was performed in triplicate
615 in a total volume of 10 µL (0.4 µM of each forward and reverse primer; 5 µM 1x SYBR® Select
616 Master Mix, Applied Biosystems; 1 µL DNA). Each DNA sample was screened with two different
617 sets of primers targeting either the actin gene of *A. mellifera*, or the universal 16S rRNA region.

618 For each target, standard curves were generated for absolute quantification using serial dilutions
619 (from 10^7 to 10 copies) of the target amplicon cloned into the plasmid vector. Absolute abundance
620 of bacteria was calculated by using the standard curve and were normalized by the median actin
621 copy number per condition (to account for differences in gut size) and by the amount of 16s rRNA
622 copies per genome. For the calculation we used the following formula:

623 $$Absolute\ bacterial\ abundance = 10^{\left(\frac{Ct_{target} - Intercept}{Slope}\right)} * dilution\ factor\ \div number\ of\ 16S\ rRNA\ copies \div$$
624 $$(median\ of\ actin\ copies\ per\ condition)$$

625 Here, Ct_{target} is the cycle threshold of the target bacterium and intercept and slope correspond to
626 the values calculated for the standard curve of the target bacterium.

627 **Single cell microscopy**

628 *F. perrara* was freshly grown from stock on plate. Subsequently, liquid overnight cultures starting
629 at an OD_{600} 0.1 were inoculated in TYG for the experiment of the Figure 1 – figure supplement 2,
630 and in BHI for the experiment of the Figure 6 – figure supplement 3. Liquid cultures were grown
631 overnight 16-24 hours with shaking at 34-35 °C in a ThermoMixer C (Eppendorf) in anaerobic
632 atmosphere. For Figure 1 – figure supplement 2, OD_{600} was measured and adjusted to 0.1 – 0.01
633 and cells were distributed onto small agar patches on a microscopy slide (Milan S.A., Menzel-
634 Gläser). Cells were observed under 1000 times magnification using a ZEISS imager M1
635 microscope with phase contrast (PH3) condenser. Pictures were acquired randomly on the slides
636 with VisiView software, 8-bit images were corrected with ImageJ and the contrast was set at min-
637 value of 0 and max-value of 4000. A 10 µM scale bar was added with ImageJ (76). For the
638 experiment displayed in Figure 6 – figure supplement 3, OD_{600} was adjusted to 0.1 and 10µl of
639 bacterial solution were distributed onto small patches containing BHI and 1.5% UltraPure™
640 Agarose from Invitrogen™. Images were obtained using a Nikon ECLIPSE Ti Series inverted
641 microscope coupled with a Hamamatsu C11440 22CU camera and a Nikon CFI Plan Apo Lambda
642 100X Oil objective (1000x final magnification). A 20 µM scale bar was added with ImageJ. For
643 both experiments, the MicrobeJ plugin for ImageJ was used to measure cell size and area using
644 the acquired pictures (77).

645

646 **Isolation and identification of aryl polyene compounds**

647 *F. perrara* was streaked from the -80 °C glycerol stock onto mTYG plates. Plates were placed in
648 an anaerobic tank with a pack of AnaeroGel 3.5 L (AN0035A Thermo Scientific) at 37 °C and
649 incubated. Under aerobic sterile conditions, colonies were picked and 5 mL of mTYG medium
650 were inoculated in a Hungate tube. After purging the liquid for 1 h with gas (83% N_2, 10% CO_2,
651 7% H_2 v/v) bacteria were grown at 37 °C. After one day of growth, *F. perrara* wt and the *ihfA**
652 mutant were individually cultivated in Hungate tubes containing 30 mL mTYG for three days.
653 Pellets were harvested, extracted with dichloromethane and methanol, then extracts were
654 analyzed by HPLC-HESI-HRMS. The data revealed a strongly UV-Vis absorbent ion peak at *m/z*

655 323.1647 $[M+H]^+$. To enrich this compound, 400 mL of mTYG were inoculated with 1 mL of pre-
656 culture in a Hungate tube and purged as described above. After 5-10 days all but a few mL of
657 medium were harvested and 400 mL of fresh mTYG was added under sterile aerobic conditions,
658 purged with anaerobic gas and incubated at 37 °C. A total of 3 L of mTYG were used to obtain
659 6.53 g of cells, which were stored at -80 °C. Light exposure was minimized during all following
660 steps of the aryl polyene enrichment procedure. A mixture of 340 mL dichloromethane and 170
661 mL of methanol was added to *F. perrara* cell pellets. After 2 h stirring at room temperature (RT),
662 the suspension was filtered and 250 mL KOH (0.5 M) were added. After an additional 1 h of stirring
663 at RT the pH was set to 6 using H_2SO_4 (1 M). The organic layer was washed twice with 500 mL
664 water, once with 250 mL brine, dried over Na_2SO_4 and concentrated. The extract was separated
665 by reverse-phase high performance liquid chromatography (RP-HPLC , Phenomenex Luna 5 µm
666 C18, φ 21.2 x 250 mm, 15.0 mL/min, λ=420 nm) with water +0.1% formic acid (solvent A) and
667 MeCN +0.1% formic acid (solvent B). Solvent compositions of 5% B for 4 min, a gradient to 95%
668 B for 18 min, 95% B for 9 min and 5% B for 4 min were used. Fractions around 24 min exhibited
669 strong UV absorption at 420 nm and were further purified by RP-HPLC (Phenomenex Luna 5µ
670 Phenyl-Hexyl, φ 10 x 250 mm, 2.0 mL/min, λ=420 nm) with 80% B for 5 min and a gradient of
671 80% B to 100% B for 30 min. Peaks around 17 min were combined, concentrated and analyzed
672 by NMR spectroscopy. HPLC-HESI-HRMS was performed on a Thermo Scientific Q Exactive
673 mass spectrometer coupled to a Dionex Ultimate 3000 UPLC system. NMR spectra were
674 recorded on a Bruker Avance III spectrometer equipped with a cold probe at 500 MHz and
675 600 MHz for ^{1}H NMR and 125 MHz and 150 MHz for ^{13}C NMR at 298 K. Chemical shifts were
676 referenced to the solvent peaks of DMSO-d_6 at δ_H 2.50 ppm and δ_C 39.51 ppm.

677

678 **Structural characterization of the aryl polyene**

679 ^{1}H NMR in conjunction with HSQC data suggested approximately 15 methines and aromatic
680 protons, one methoxy group and one methyl group (**Figure 2 - figure supplement 3 - 7**). From
681 the COSY spectrum, four methines of the conjugated double bond system, and two of the aromatic

682 protons could be connected (**Figure 2 - figure supplement 7 and 8**). HMBC correlations from
683 the methyl group to an aromatic carbon at δ_C 156 ppm placed it in *ortho*-position of a hydroxy
684 group and next to a singlet aromatic proton. The singlet of the methoxy-group was connected to
685 a carbonyl group by HMBC correlations (**Figure 2 - figure supplement 9**).

686

687 **Construction of gene deletion mutants**

688 Targeted in-frame gene deletions of *F. perrara* were constructed using a two-step homologous
689 recombination procedure (see **Figure 6 – figure supplement 1**). In a first step, suicide plasmids
690 were constructed harboring two adjacent 700-800 bp-long homology regions matching the up-
691 and downstream region of the gene or gene cluster to be deleted. To this end, the two homology
692 regions were amplified using 2 Phanta Max Master Mix (Vazyme) and cloned into pKS2 using
693 Golden Gate assembly. pKS2 is a derivative of pSEVA312 (78) which contains a sfGFP
694 expression cassette flanked by two BsaI restriction sites in the multiple cloning site. All clonings
695 were done in *E. coli* DH5a/λpir. To validate successful cloning of the two homology regions, PCR
696 and Sanger sequencing was performed. The plasmids derived from pKS2 containing the
697 homology regions were shuttled into the diaminopimelic acid (DAP)-auxotroph *E. coli* JKE201 and
698 delivered to *F. perrara* wt via conjugation using bi-parental mating. To this end, *E. coli* JKE201
699 carrying the plasmid of interest was cultivated for 16-20 hours at 37 °C in LB with 500µM DAP
700 (Sigma, LB-DAP) and 30 µg/ml Chloramphenicol. Sub-cultures were made by diluting the culture
701 at a ratio of 1:20 into fresh medium and incubated until exponential growth was reached. A fresh
702 culture of *F. perrara* was prepared by growing it for 36 h on mTYG agar. *F. perrara* and *E. coli*
703 were harvested in PBS and the OD_{600} adjusted to 10. Equal quantities of both bacteria were mixed
704 and spotted onto a cellulose acetate membrane filter (0.2 µm, 25 mm, Huberlab, Sartorius) placed
705 on BHI agar with 500 µM DAP, followed by incubation at 35 °C for 6 hours under microaerophilic
706 condition. Filters with bacterial mixtures were removed from the plates with a forceps, placed into
707 a tube with PBS. Bacteria were removed from the filter by pipetting, vortexing and agitation for 10
708 min at 1500 rpm (Thermomixer C, Eppendorf). The bacterial suspension was centrifuged at 8000x

709 g for 10 minutes, the supernatant discarded to remove dead bacteria and the bacterial pellet was
710 washed once with 1000 µl PBS before resuspending in a reduced volume, i.e. 100 µl PBS. The
711 bacterial mixture was plated onto CBA and mTYG with selection antibiotic and incubated at 35 °C
712 for 5 days under anaerobic condition. Colonies were picked after 4-5 days of incubation and
713 expanded to fresh plates. DNA was isolated and five different PCRs performed to check for
714 successful integration of the plasmid into the chromosomal region of *F. perrara* targeted for
715 deletion. Positive clones (loop-in strains) were stocked in liquid mTYG containing 20% (v/v)
716 glycerol at -80 °C until further usage. To select for bacteria that have lost the integrated plasmid,
717 *F. perrara* loop-in strains were grown on mTYG agar and subsequently transformed with plasmid
718 pYE1. pYE1 is a derivative of pBZ485 (79) containing the restriction enzyme *I-SceI* under the
719 control of the IPTG-inducible *lac* promoter. The activity of the restriction enzyme *I-SceI* will
720 negatively select bacteria containing pKS2-derivatives as two *I-SceI* sites are flanking the multiple
721 cloning sites on pKS2. To generate electrocompetent *F. perrara* cells, the bacteria were cultivated
722 from glycerol stocks on mTYG agar and incubated at 35 °C for 2 days under anaerobic condition.
723 Bacteria from plate were inoculated in BHI broth with a starting OD_{600} of 0.1 and grown
724 anaerobically at 40 °C for 12-16 hours. Subsequently, growth was stopped by placing cultures
725 onto ice for 15 minutes. Cells were made electrocompetent by washing twice with ice-cold MOPS
726 solution supplemented with 20% glycerol, with decreasing volumes per wash. Electrocompetent
727 cells were mixed with >500 ng plasmid DNA and incubated for 15 minutes on ice before
728 transferring into an electroporation cuvette. Electroporation was performed applying a voltage of
729 2.5 kV with resistance of 200 Ω and capacitance of 25 µF. Bacteria were immediately
730 resuspended in BHI and incubated anaerobically for 6 hours at 35 °C to allow phenotypic
731 expression. Bacteria were plated on CBA, mTYG and/or BHIA plates with 25 µg/ml Kanamycin
732 and 100 µM IPTG to select for pYE1 and induce the restriction enzyme *I-SceI*. Plates were
733 incubated in anaerobic atmosphere at 35 °C. After 3 to 5 days of incubation, bacterial colonies
734 were replica plated onto fresh plates containing 15 µg/ml chloramphenicol (selection marker of
735 pKS2-derivatives) or 25 µg/ml kanamycin (selection marker of pYE1) to identify clones that cannot
736 grow on chloramphenicol anymore as a consequence of the loss of the integrated pKS2-

737 derivative. DNA was extracted and a PCR screen performed with primers amplifying the gene
738 targeted for deletion as well as the overspanning region of the deletion. All clones possessing the
739 gene deletion were subsequently expanded on mTYG agar and stocked in glycerol as described
740 above

741

742 **Correspondence between OD and CFU**

743 For the wt, *ihfA** and the six gene-deletion mutants, bacteria were grown in BHIA plates for 3 days
744 at 35ºC in anaerobic conditions. On the day of the experiment, bacteria were harvested and a
745 bacterial solution at OD_{600} =0.1 was prepared per each genotype. Serial dilutions were performed
746 in a 96-well plate by transferring 10µl of OD_{600} =0.1 into 90µl of BHI medium followed by several
747 1:10 dilutions in BHI. For each genotype, 5 µl of all dilutions were plated on BHIA plates, incubated
748 for 3 days at 35ºC in anaerobic conditions and quantified to calculate the number of CFUs present
749 in 5 µl of the initial OD_{600} =0.1 solution. The CFU values present in 5 µl of bacterial solution at
750 OD_{600} =0.1 is of relevance as it corresponds to the volume fed to bees in the colonization
751 experiments. Three experimental replicates were performed.

752

753 **Growth curves in liquid cultures**

754 *F. perrara* was freshly grown from stock on BHIA plates. Subsequently, liquid overnight cultures
755 starting at an OD_{600} =0.1 were inoculated in BHI and grown for 16-24 hours anaerobically with
756 shaking at 35 °C and 600 rpm in a ThermoMixer C (Eppendorf) in anaerobic atmosphere. To
757 obtain the growth curves, one 96-well plate was inoculated with different *F. perrara* strains. Each
758 well contained 200µl of a bacterial solution at OD_{600} =0.05. Per strain, four wells were inoculated.
759 Absorbance values were measured at 600nm every 20 minutes for 72 hours, using a BioTek™
760 Epoch2 microplate reader. The plate was incubated in anaerobic conditions at 34ºC and
761 continuous orbital shaking for the duration of the experiment.

762

763 **FISH microscopy**

764 Tissue sections and FISH experiments were performed as previously described (34). Briefly, the
765 pylorus and ileum of gnotobiotic bees were dissected and fixed for five days in Carnoy's solution
766 (ethanol-chloroform-acetic acid, 6:3:1 [vol/vol]). Fixed tissue samples were washed three times
767 for 1 hour in absolute ethanol, then incubated three times for 20 min in xylene, and finally infiltrated
768 with paraffin three times for 1 hour at 60°C. Samples were placed into molds containing melted
769 paraffin and then hardened by placing them into an ice slurry. Paraffin-embedded tissues were
770 cut into serial 5-µm sections with a microtome (Leica), placed on coated microscopy slides, and
771 cleared from paraffin with xylene. Sections were then hybridized overnight with fluorochrome-
772 labeled oligonucleotide probes targeting the 16S rRNA of *F. perrara* and DAPI. Samples were
773 imaged using the Zeiss LSM900 confocal microscope. Per bacterial genotype, one gut was
774 processed and imaged. The *F. perrara* probe used is named PE1_TYE563_G2, has the sequence
775 CCGCTCCAGCTCGCACCTTCGCT and a Cy3 flurophore.

776

777 **Electron Microscopy**

778 The wt, *ihfa** and *ΔpilE* strains were grown in BHIA plates for 3 days at 34°C in anaerobic
779 conditions. The day before image acquisition, bacteria were harvested from the plates, transferred
780 to liquid BHI at an initial OD_{600} =0.1 and were grown for 16 hours in anaerobic conditions with
781 shaking. On the day images were acquired, bacteria were diluted 50 times. Each bacteria
782 suspension was adsorbed on a glow-discharged copper 400 mesh grid coated with carbon (EMS,
783 Hatfield, PA, US) during one minute at room temperature. Posteriorly, the meshes were washed
784 with three drops of distilled water and stained for one minute with uranyl acetate (Sigma, St Louis,
785 MO, US) at a concentration of 1%. The excess of uranyl acetate was drained on blotting paper
786 and the grid was dried during ten minutes before image acquisition. Micrographs were taken with
787 a transmission electron microscope Philips CM100 (Thermo Fisher Scientific, Hillsboro, USA) at
788 an acceleration voltage of 80kV with a TVIPS TemCam-F416 digital camera (TVIPS GmbH,
789 Gauting, Germany).

790

791 **Generation of the BeeComm_002 bacterial community**

792 Thirteen bacterial isolates that represent the most abundant species found in the bee gut were
793 grown individually and assembled together to generate a bacterial community named
794 **BeeComm_002** (**Supplementary Table 4**). Each individual member was grown in agar plates of
795 its respective preferential medium and culture conditions for 3 days, bacteria were harvested from
796 the plates, diluted to OD_{600} =1 in PBS, mixed together in the same proportions and placed in a
797 glycerol stock (20% final concentration) at -80ºC. *Gilliamella* strains were grown in BHIA plates
798 and incubated in anaerobic conditions at 35ºC. *Bifidobacterium*, *Lactobacillus* and
799 *Commensalibacter* strains grew anaerobically and at 35ºC in Man, Rogosa and Sharpe agar
800 plates supplemented with fructose and L-cysteine. *Snodgrassella alvi* was grown in Trypticase
801 Soy agar plates, *Bartonella apis* grown in Columbia Broth agar plates supplemented with 5%
802 sheep blood and both isolates were placed in micro-aerophilic conditions with 5% CO2 and at
803 34ºC.

804

805 **Co-colonization of bees with *F. perrara* and BeeComm_002**

806 Each gene-deletion mutant, the wt and the *ihfA** mutant of *F. perrara* were grown as previously
807 mentioned and diluted to OD_{600} =1 on the day the colonization experiment was performed. 100 µl
808 of a given *F. perrara* genotype at OD_{600} =1, 100 µl of BeeComm_002 at OD_{600} =1 and 800 µl of a
809 PBS and sugar water solution (1:1) were mixed together. As BeeComm_002 is composed of 13
810 isolates and was mixed in a 1 to 1 ratio with *F. perrara*, *F. perrara* was 13 times more abundant
811 than any individual member of this synthetic community. For the control treatments where
812 BeeComm_002 was not added (mono-associations), 100 µl of a given *F. perrara* genotype at
813 OD_{600} =1 were diluted in 900 µl of a PBS and sugar water solution (1:1). Gnotobiotic bees were
814 generated, manipulated and inoculated with bacteria as previously mentioned. Ileum/pylorus
815 regions were dissected at day 10 after inoculation and scab formation was assessed before snap-
816 freezing the samples in liquid nitrogen. Samples were placed at -80ºC until DNA was extracted

817 using previously mentioned methods. Bacterial abundance was quantified using the approach
818 described in the Methods section "Bacterial quantification by qPCR". Primers used in this
819 experiment are found in **Supplementary Table S3.**
820

821 **Genome re-sequencing**

822 All gene deletion strains and the three white variants of *F. perrara* PEB091 were subjected to
823 Illumina genome re-sequencing at Novogene (2x150bp). Mutations in the re-sequenced genomes
824 relative to the genome of the wt strain of *F. perrara* were analyzed with *breseq* (80). The detailed
825 results of this analysis can be found: https://drive.switch.ch/index.php/s/kCNTp4g7n60ffMi.

826

827 **Statistical analysis**

828 Statistical analysis was performed using GraphPad Prism v6.01 or R. Results of all statistical tests
829 can be found in **Supplementary Dataset 5**. Normality was analyzed using D'Agostino-Pearson
830 and/or Shapiro-Wilk test. For comparison with two conditions, t-test was used for parametric data
831 and Wilcoxon sum-rank test or Kolgomorov-Smirnov test for non-parametric data. For comparison
832 of the growth curves of *F. perrara* wt and *ihfA**, we used a permutation test
833 'compareGrowthCruves' included in the statmod package of R (81). For the analysis of the CFU
834 counts, a linear model with binomial distribution was calculated with CFUs as the dependent
835 variable and Genotype and Experimental Replicate as independent variables. Post-hoc
836 comparisons between genotypes were performed using the emmeans R package (https://cran.r-
837 project.org/web/packages/emmeans/index.html). For the comparison of the cell lengths, Wilcoxon
838 sum-rank test was performed.

839

840 **Data availability**

841 RNA sequence datasets are available under NCBI Gene Expression Omnibus ID GSE189728.
842 Code, scripts and numeric data files of experimental data have been deposited on Switchdrive:
843 https://drive.switch.ch/index.php/s/kCNTp4g7n60ffMi.

844

845 **Acknowledgments**

846 We thank Stephan Gruber for input regarding the characterization of the ihfA* mutant strain and
847 general feedback for the manuscript. We are grateful to Nicolas Neuschwander and Lucie Kesner
848 for helping with some of the bee experiments. We thank Tania Trabajo for her help with the single
849 cell imaging. This project was funded by the ERC-StG 'MicroBeeOme' (grant agreement No.
850 714804), the Swiss National Science Foundation (grant agreement No. 31003A_160345 and
851 31003A_179487), the NCCR Microbiomes (all awarded to PE). J.P. acknowledges funding by the
852 European Research Council (ERC) under the European Union's Horizon 2020 Research and
853 Innovation Program (grant agreement No. 742739).

854

855 **Figures**

856

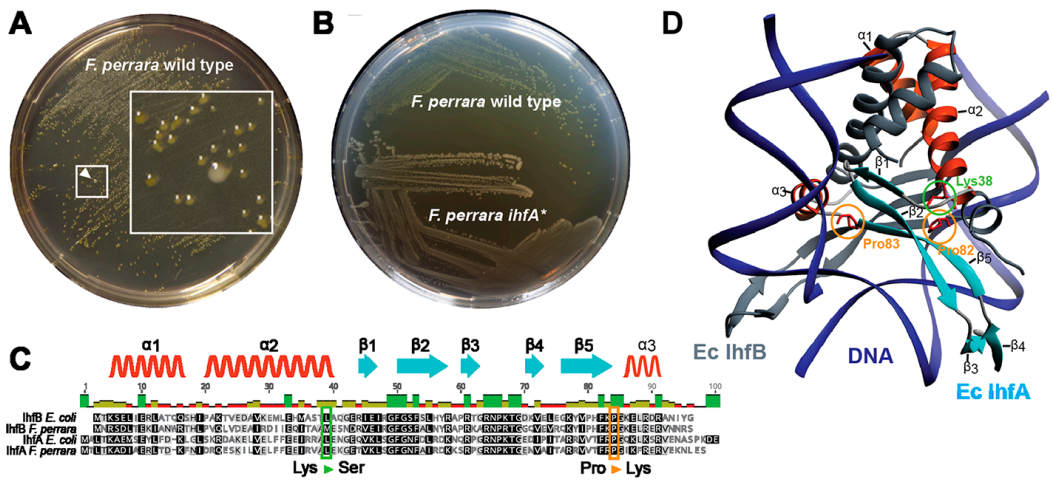

857

858 **Figure 1. Isolation of a spontaneous *ihfA** mutant of *F. perrara* displaying an altered colony**
859 **morphotype. (A)** Colonies of *F. perrara* PEB0191 (wt) after 48 hours of growth on mTYG agar.
860 Arrowhead points at a larger white colony in between many yellow colonies. The area in the white
861 square is magnified. (**B**) Colony morphology of *F. perrara* wt and the isolated white *ihfA** mutant
862 after growth on mTYG for 48 hours. (**C**) Protein sequence comparison of IhfA and IhfB of *F.*
863 *perrara* wt and *E. coli* wt. The outlined positions refer to the residues mutated in the three
864 spontaneous *ihfA* mutants: (i) lysine (Lys) to serine (Ser) at position 38 of *F. perrara* IhfA, (ii)
865 proline (Pro) to lysine (Lys) at position 83 of *F. perrara* IhfA, (iii) proline (Pro) to lysine (Lys) at
866 position 82 of *F. perrara* IhfB. Note that the numbers given on top of the alignment refer to
867 alignment positions and not to positions in the individual sequences. Secondary structures are
868 depicted above as ribbons (α-helix) and arrows (β-sheet) and are numbered according to their
869 appearance in the protein and the structure shown in D. (**D**) Three-dimensional structure of *E. coli*
870 IhfA/B heterocomplex with DNA (source protein databank NDB: PDT040). DNA is depicted in blue
871 and IhfB in dark grey. IhfA is colored according to secondary structure: α-helix orange, β-sheet
872 light blue and the rest in light grey. α-helices and β-sheets are numbered. The mutated Pro83 and
873 Lys38 residues of *F. perrara* IhfA and the Pro82 residue of IhfB are marked with an orange and

874 green circle, respectively.

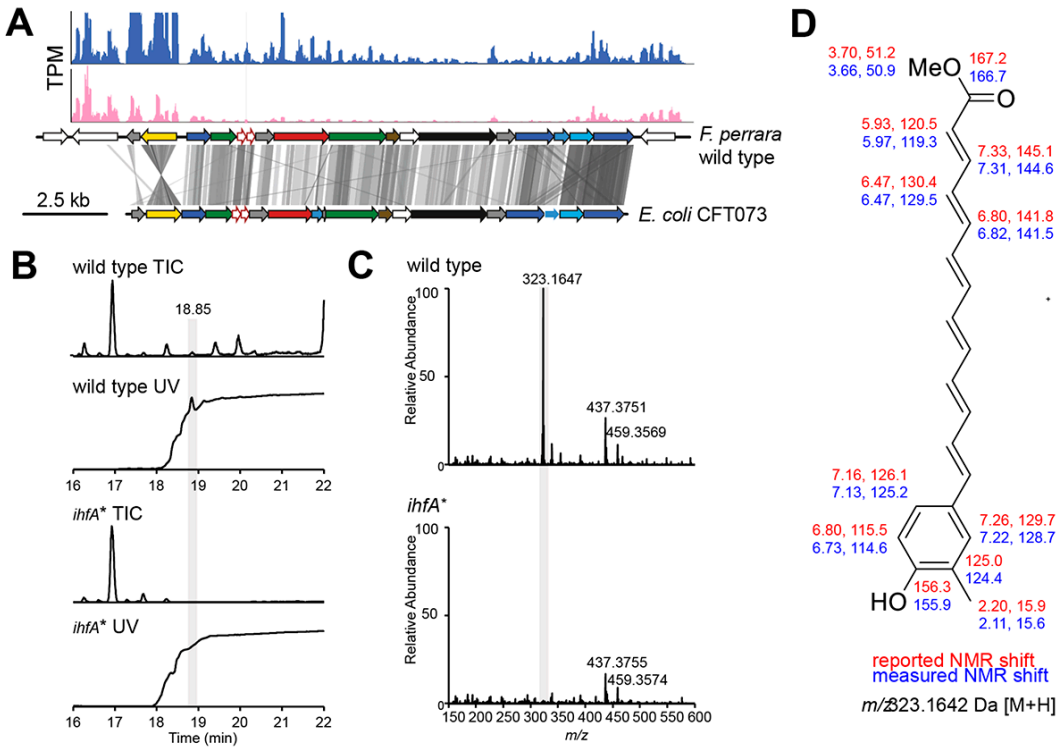

875

876 **Figure 2. Metabolite analysis of *F. perrara* wt and the *ihfA** mutant. (A)** Comparison of gene
877 synteny and sequence similarity of the genomic islands of *F. perrara* PEB0191 (top) and *E. coli*
878 CFT073 (bottom) encoding the aryl polyene (APE) biosynthesis genes. Grey lines indicate
879 homologous regions based on tblastx analysis. Plots were generated with genoplotR (82).
880 Transcripts per million (TPMs) are shown on top of the genomic island for one RNAseq replicate
881 of each *F. perrara* wt (blue) and the *ihfA** mutant grown in vitro. Coverage plots were generated
882 with the Integrated Genome Browser v9 (74). (**B**) Total ion chromatogram (TIC) and UV trace
883 (λ=420 nm) of wt and *ihfA**. A peak highly abundant in the wt was discovered at 18.85 min. Its
884 high UV absorbance at λ=420 nm indicated a conjugated carbon double bond system. (**C**) The
885 normalized mass spectrum at 18.85 min reveals the ion *m/z* = 323.1647 Da to be approximately
886 50-fold more abundant in the wt compared to *ihfA**. (**D**) Enrichment of the ion containing fraction
887 by HPLC followed by NMR experiments suggest a structure identical to that reported by (43).
888 Reported (red) and observed (blue) ^{1}H and ^{13}C chemical shifts are shown. Central methines could
889 not be assigned.

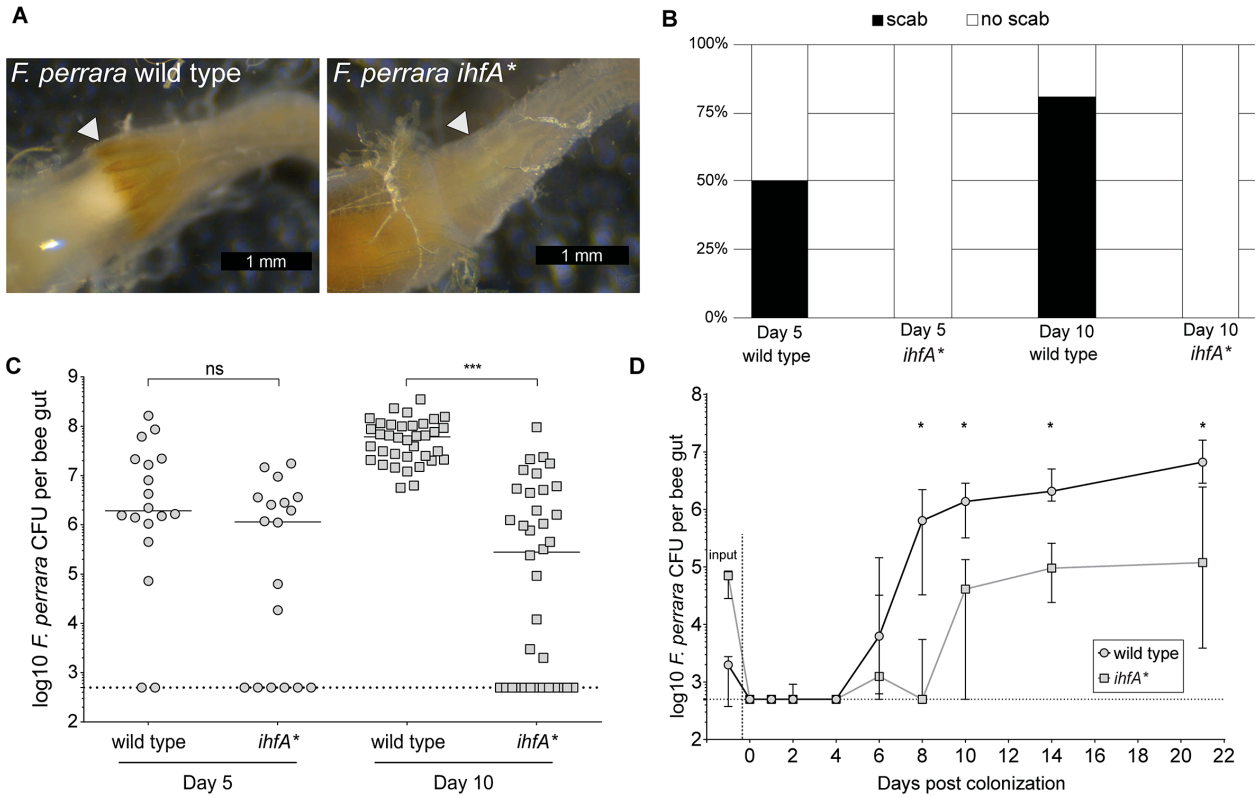

Figure 3. *F. perrara ihfA mutant displays a colonization defect. (A)** Light microscopy pictures of pylorus region of bees colonized with *F. perrara* PEB0191wt or *ihfA** 10 days post colonization. (**B)** Quantification of scab phenotype of bees 5 and10 days post colonization with n=18 and n=36 per treatment, respectively. (**C)** Quantification of colonization levels are measured by colony forming units (CFUs) at day 5 (n=18) and day 10 (n=36) post colonization. Wilcoxon rank-sum test was used to assess significant differences. (**D)** Time course experiment of bees colonized with *F. perrara* wt or *ihfA**. Colonization levels were measured by CFUs every second day until day 10 and then at day 14 and day 21. n=12 bees per time point per treatment. Wilcoxon rank-sum test was used to assess significant differences per time point. Error bars represent median and interquartile range. Data from three independent experiments. *p<0.05, **p<0.01, ***p<0.001.

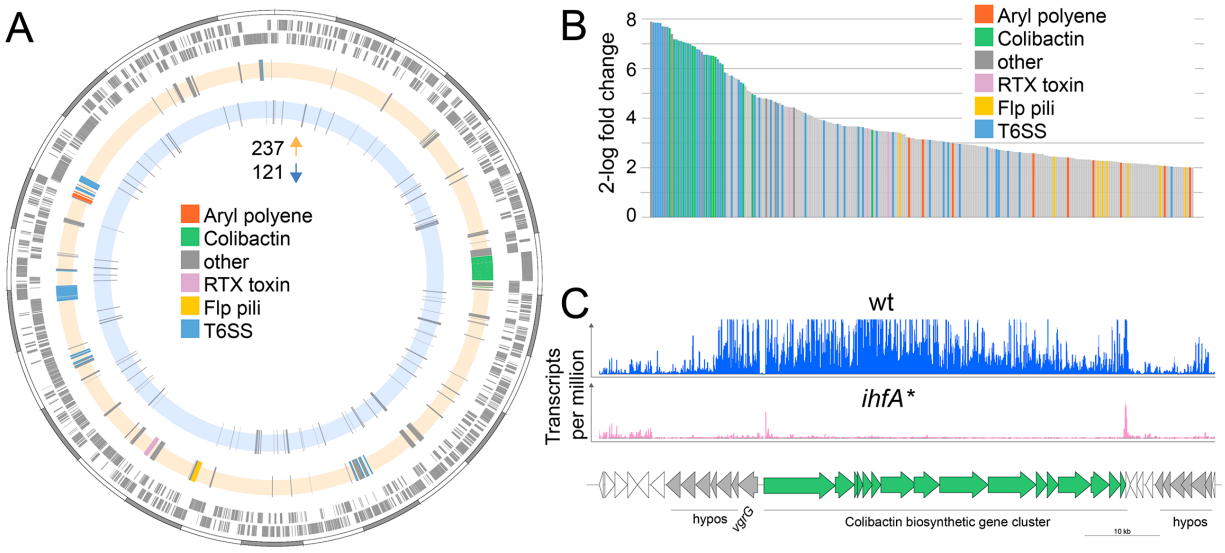

Figure 4. Differential gene expression between *F. perrara* wt and *ihfA mutant during *in vitro* growth**. (**A)** Chromosomal localization of all genes significantly differentially expressed (2-log fold change = |2|, Fisher's exact test p value <0.05, FDR <0.05) between *F. perrara* wt and the *ihfA** mutant. Starting from outside, the first circle shows the scale of the genome representation of *F. perrara* in gray and white steps of 100 kb. The second and third circles (gray) depict the genes on the plus and minus strands of *F. perrara*. The fourth (beige) and fifth (light blue) circle depicts genes upregulated and downregulated in wt compared to *ihfA**. Genomic islands are highlighted by coloration. (**B)** Bar plot of the genes differentially expressed between *F. perrara* wt and *ihfA** with a log2-fold change >2 (Fisher's exact test p value <0.05, FDR <0.05). (**C)** Comparison of the transcriptional profile of the genomic location encoding the colibactin biosynthetic gene cluster between *F. perrara* wt and the *ihfA** mutant. Transcripts per million were visualized using the Integrative Genome Browser (74). The colibactin operon is schematically depicted below (green arrows).

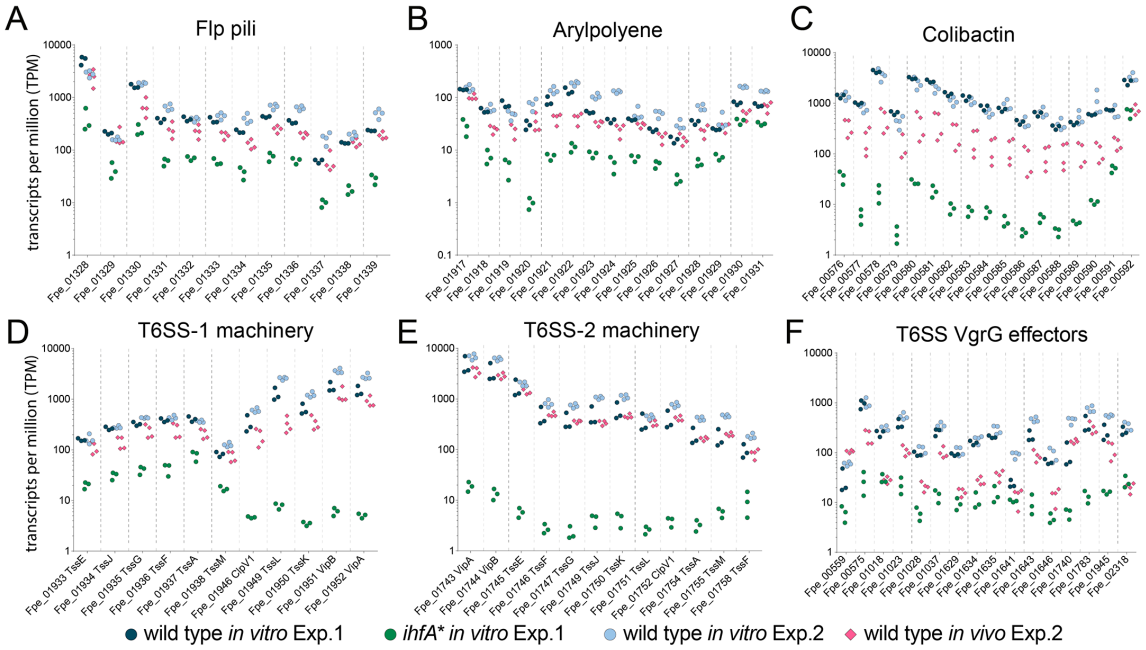

Figure 5. Gene expression of Ihf-regulated genes of *F. perrara* ten days post-inoculation of gnotobiotic honey bees. Transcripts per million were calculated for all replicates of the *in vitro* and the *in vivo* RNAseq experiments. For the in vitro experiment (Exp. 1), all three replicates of the wt and the *ihfA** mutant are shown. For the *in vivo* experiment (Exp. 2), the four replicates of the day 10 time-point and the in vitro reference condition are shown. Data for day 5 time-point in comparison to day 10 time-point is shown in **Figure 5 – figure supplement 2**.

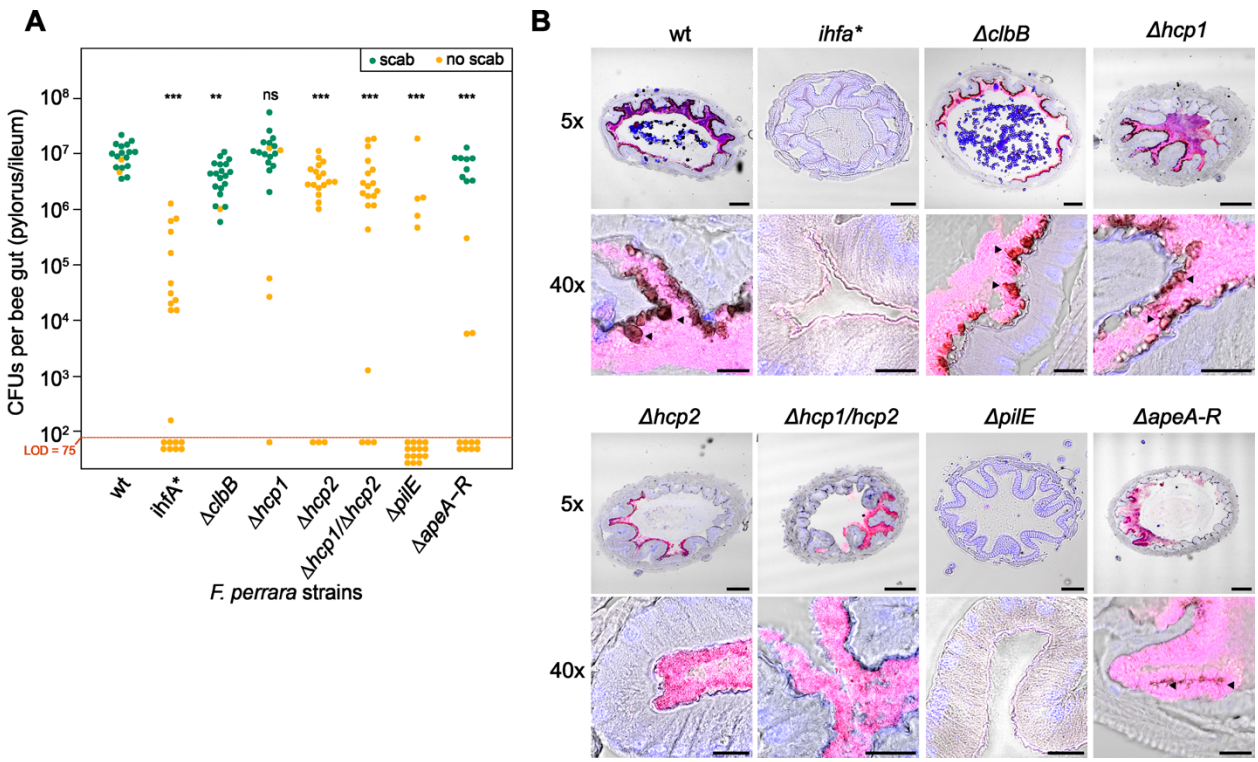

927

928 **Figure 6. Gut colonization phenotypes of different gene deletion mutants of *F. perrara.* (A)**
929 Colonization levels were assessed 10 days after inoculation by counting colony forming units
930 (CFUs) in dilutions of homogenized bee guts plated on BHI agar. Only the pylorus and ileum
931 section of the gut were analyzed. Limit of detection (LOD) corresponds to the lowest colonization
932 level detectable in our assay, i.e. points below the LOD correspond to bees for which no CFUs
933 were detected. Statistically significant differences of the colonization levels of each mutant relative
934 to the wt of *F. perrara* were determined using the Wilcoxon rank-sum test with BH correction.
935 Bees were inoculated with an OD_{600} of 0.1. Data come from two independent experiments.
936 **Supplementary Figure 15** shows the data points by experiments. * $p<0.05$, **$p<0.01$,
937 ***$p<0.001$. Filled circle colors indicate whether a scab was detected during dissection (green =
938 scab; yellow = no scab). **(B)** Location within the pylorus was assessed using FISH microscopy.
939 Bees were inoculated with different *F. perrara* genotypes at OD_{600} =0.1, guts were dissected at
940 day 10 after inoculation and sectioned using a microtome. Hybridizations were done with probes
941 specific for *F. perrara* (magenta). DAPI counterstaining of host nuclei and bacteria is shown in
942 blue. Images were generated by merging brightfield, *F. perrara* and DAPI images that were
943 obtained for the same section of the gut. The composite images here shown were obtained by

944 merging the images of each channel presented in **Figure 6 – figure supplements 6 and 7**. These
945 were obtained using the 5x and 40x objectives of the Zeiss LSM900. Scale bar for images
946 obtained with 5x: 100 µm, for 40x: 20 µm.
947
948

949

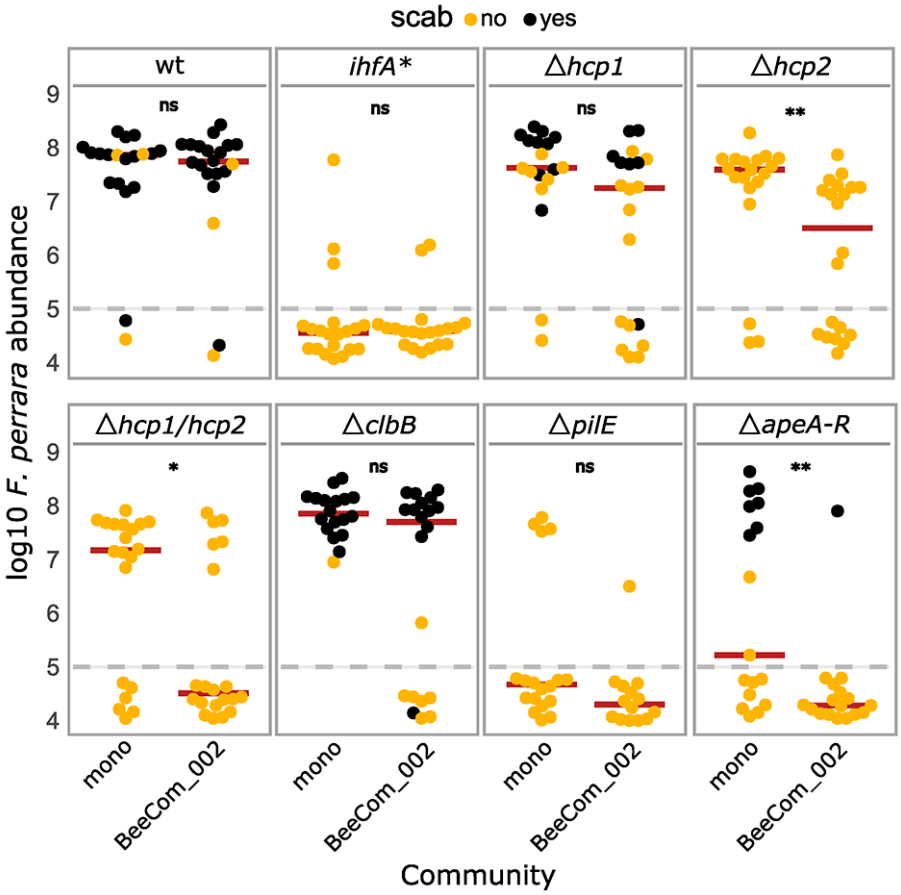

950
951 **Figure 7. Gut colonization of the gene deletion mutants in the presence of bacterial**
952 **competition.** Bees were inoculated with *F. perrara* alone (mono) or in the presence of a defined
953 bacterial community representing core members of the bee gut microbiota (BeeCom_002).
954 Colonization levels were assessed 10 days after inoculation by qPCR. Only the pylorus and ileum
955 section of the gut were analyzed. The dashed grey line refers to the limit of detection (LOD) and
956 corresponds to the lowest colonization level detectable in our assay, i.e. points below the LOD
957 correspond to bees for which no *F. perrara* was detected. Statistically significant differences
958 between the colonization levels of each mutant in mono association compared to in the presence
959 of the defined microbial community were determined using the Wilcoxon rank-sum test with BH
960 correction. Data comes from two independent experiments. **Figure 7 – figure supplement 1A**
961 shows the data points colored by experiments. * $p<0.05$, ** $p<0.01$, *** $p<0.001$. Filled circle colors
962 indicate whether a scab was detected during dissection (black = scab; yellow = no scab).

963
964
965

966 **Figure Supplements**

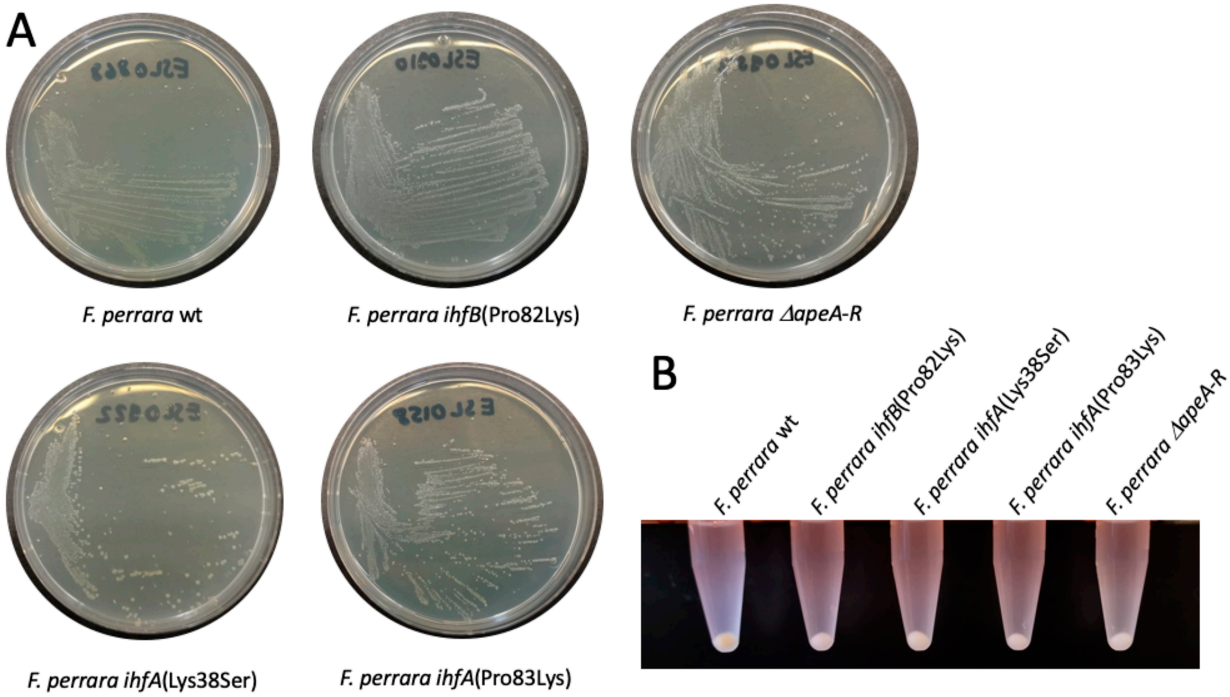

967

968 **Figure 1 – figure supplement 1. Colony morphology of different *F. perrara* strains on mTYG**
969 **agar plates. (A)** Dilution streaks of five different strains including the wt, the three separate point
970 mutation strains of IHF (two in *ihfA* and one in *ihfB*), and the *ΔapeA-R* mutant after 2 days of
971 growth under anaerobic conditions. **(B)** Bacterial cell pellets of the same strains as in **(A)**
972 harvested from the agar plates, resuspended in 1x PBS, and centrifuged for 5 min at 5000 rpm.

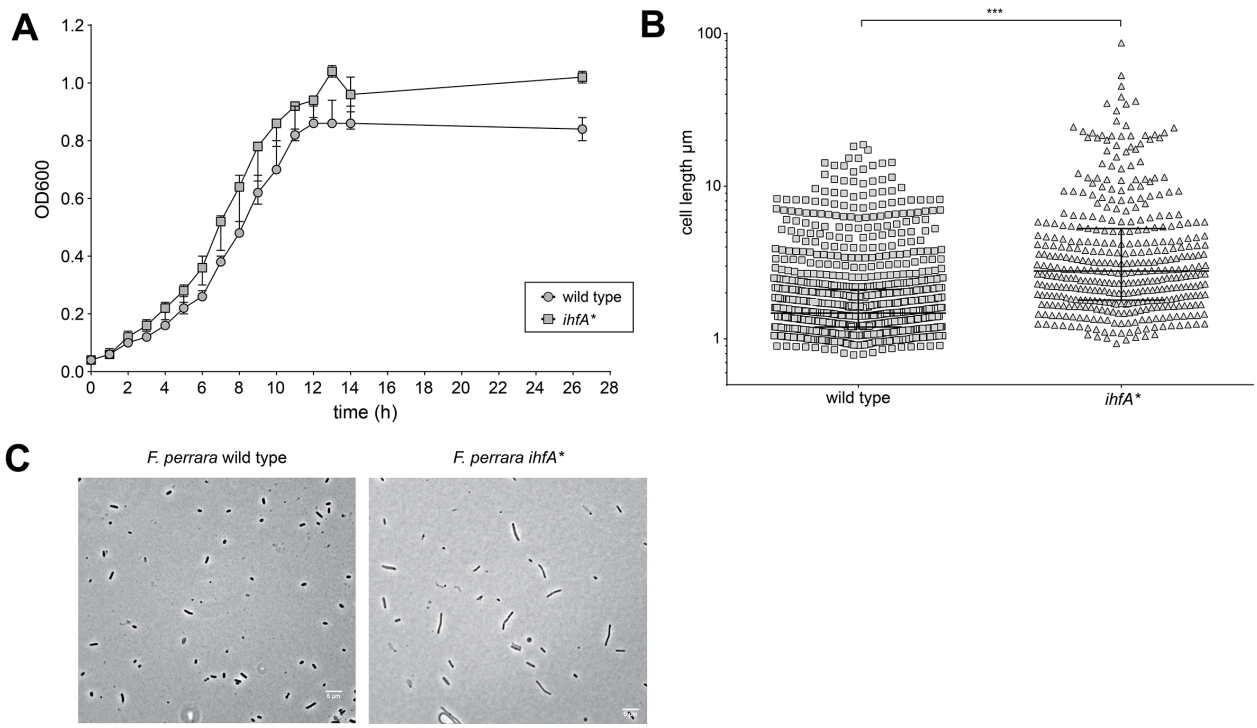

973

974 **Figure 1 – figure supplement 2. *In vitro* characterization of *F. perrara ihfA**.** **(A)** Growth curve
975 of *F. perrara* PEB0191 wt and *ihfA** in liquid TYG. The optical density (OD600) was measured
976 every hour for 14 hours (Permutation test, p = 0.097). (**B)** Quantification of single cell length of *F.*
977 *perrara* wt PEB0191 and *ihfA** from the single cell microscopy experiment shown in C.
978 Significance was tested using Kolgomorov-Smirnov test, stars depict significance: *** p<0.0001.
979 **(C)** Single cell light microscopy of *F. perrara* wt and *ihfA**. The scale bar (5µm) is depicted in the
980 right lower corner.

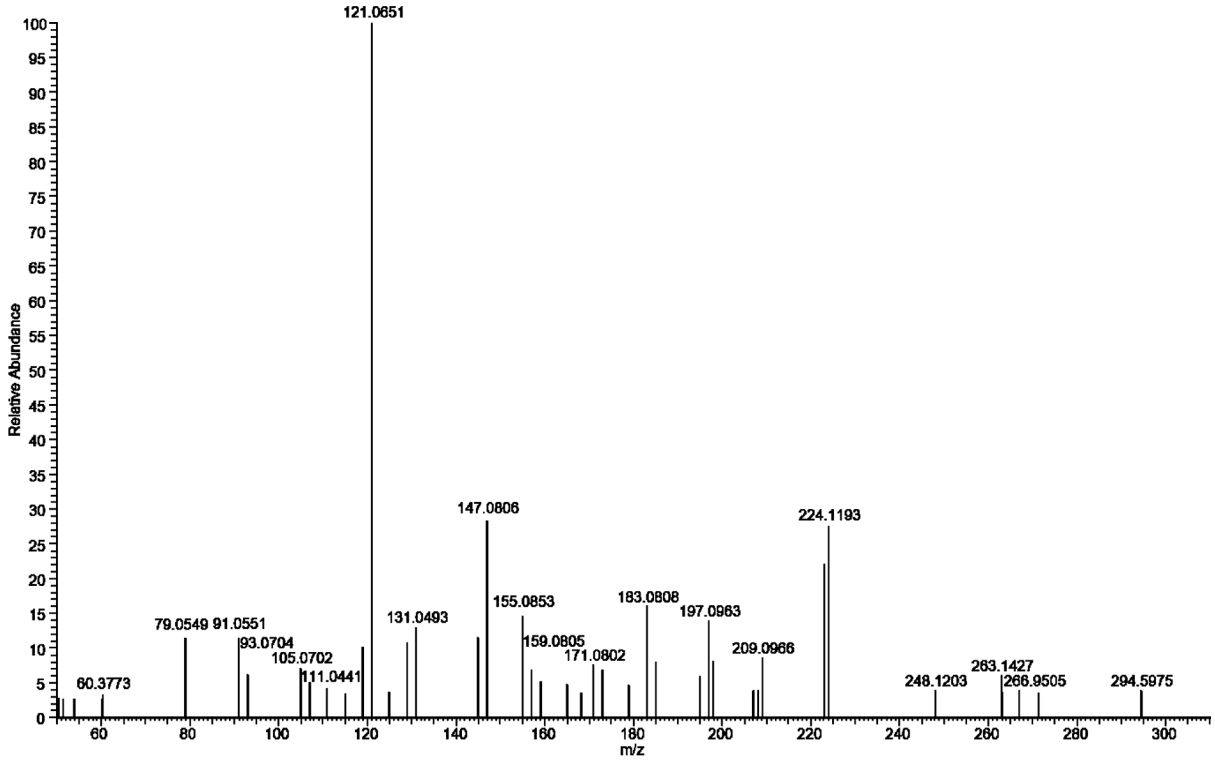

981

982 **Figure 2 – figure supplement 1. Ms-Ms fragmentation spectrum of *m/z* = 323.1647 in**
983 **extracts of *F. perrara* wt.** Many of the prominent ions were reported from aryl polyenes by **(46)**:
984 *m/z*= 121.00, 131.00, 145.00, 147.08, 171.08, 183.00, 197.08, 209.08, 223.08. The spectrum was
985 recorded at 30 kV collision energy.

986

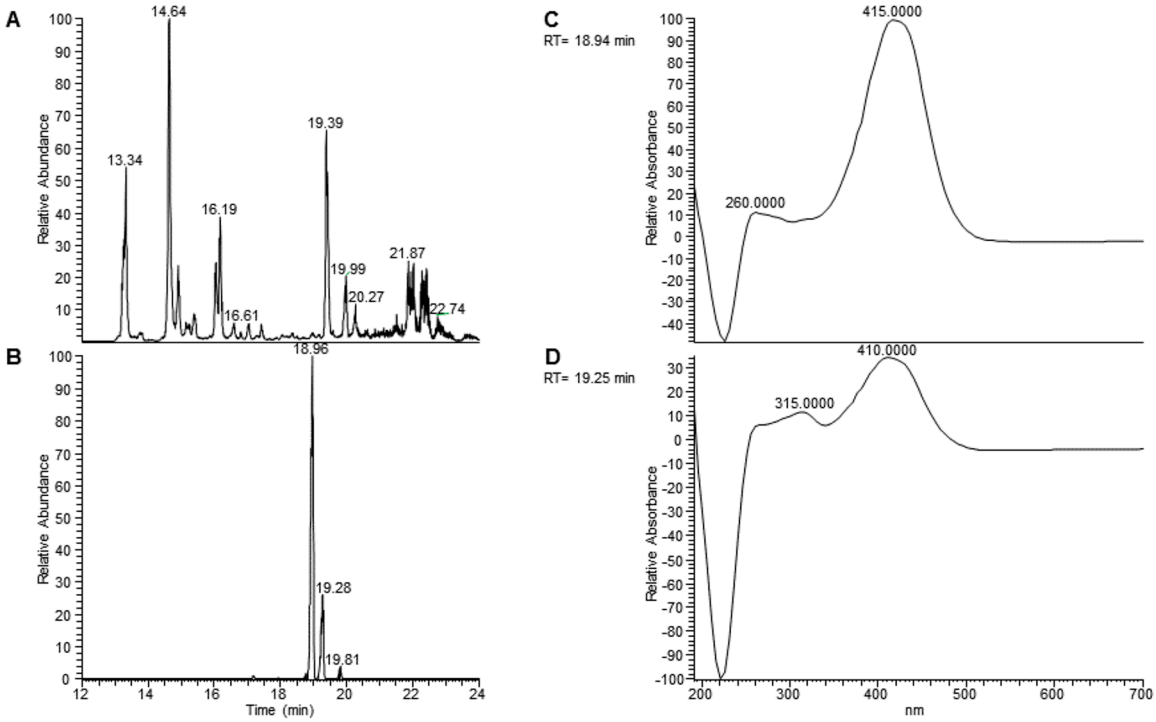

987

988 **Figure 2 – figure supplement 2**. **UV-spectrum of the extracts indicates isomerization of the**
989 **aryl polyene.** UV spectrum of the extracts indicates isomerization of the aryl polyene. (**A)** Total
990 ion chromatogram of extracts of *F. perrara* wt. (**B)** Extracted ion chromatogram of *m/z* = 323.1640
991 Da (+/- 5ppm). Storage led to the formation of an additional peak at 19.28 min, possibly by
992 isomerization. **C** The UV-spectrum at 18.94 min has the maximum around 415 nm, similar to that
993 reported by (43). **D** The UV-spectrum at 19.25 min shows an additional maximum at 315 nm,
994 characteristic for a *trans-cis* conversion of a double bond.

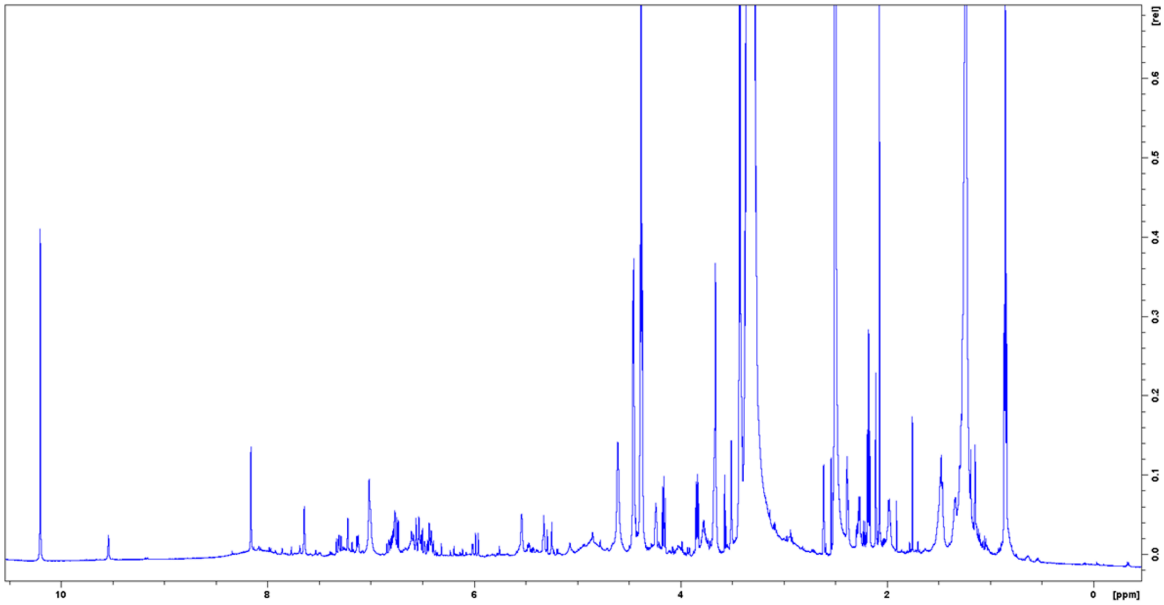

Figure 2 – figure supplement 3. ^{1}H NMR spectrum of enriched aryl polyene in DMSO–δ_6 at 298

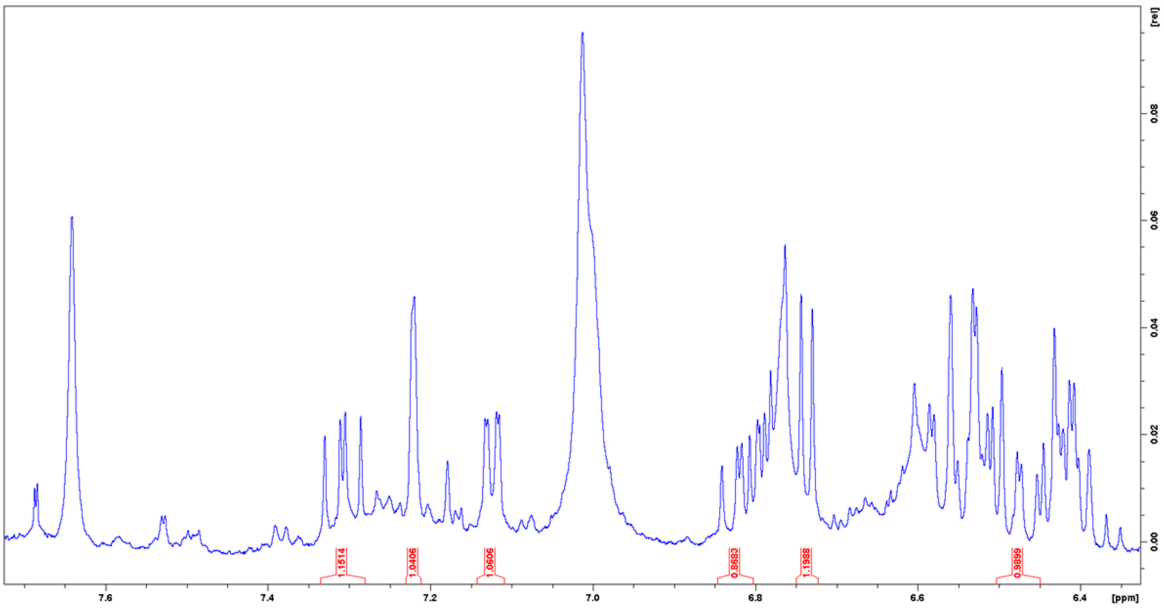

Figure 2 – figure supplement 4. ^{1}H NMR spectrum of enriched aryl polyene in DMSO–δ_6 at 298 K. Enhanced view of the aromatic region and integrals of assigned peaks.

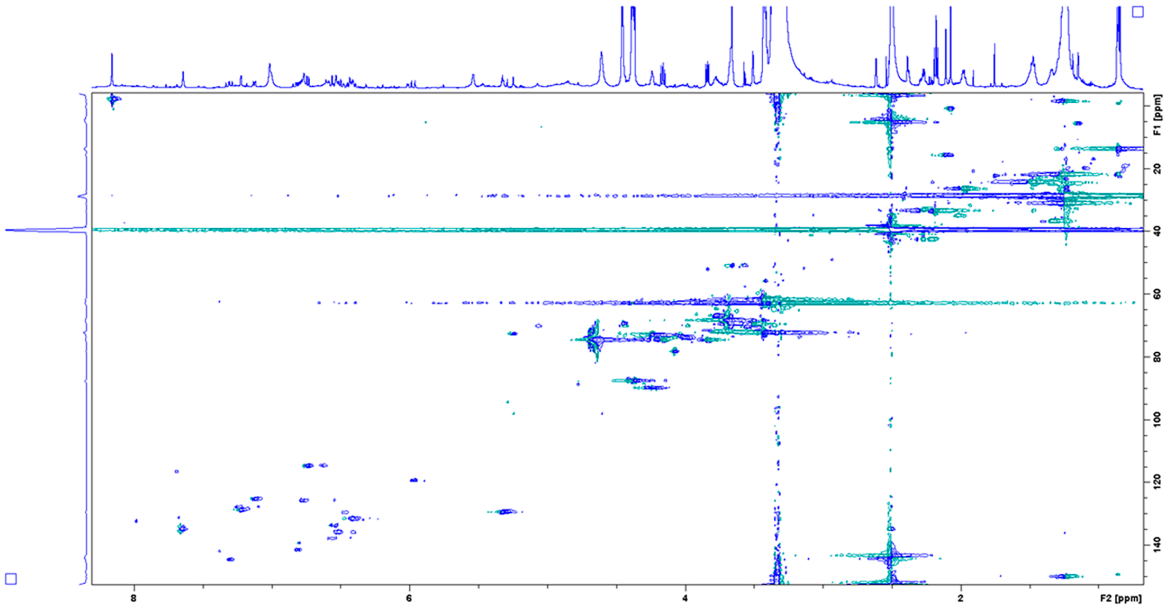

1001
1002 **Figure 2 – figure supplement 5.** HSQC spectrum of enriched aryl polyene in DMSO–δ_6 at 298 K.

1003

1004

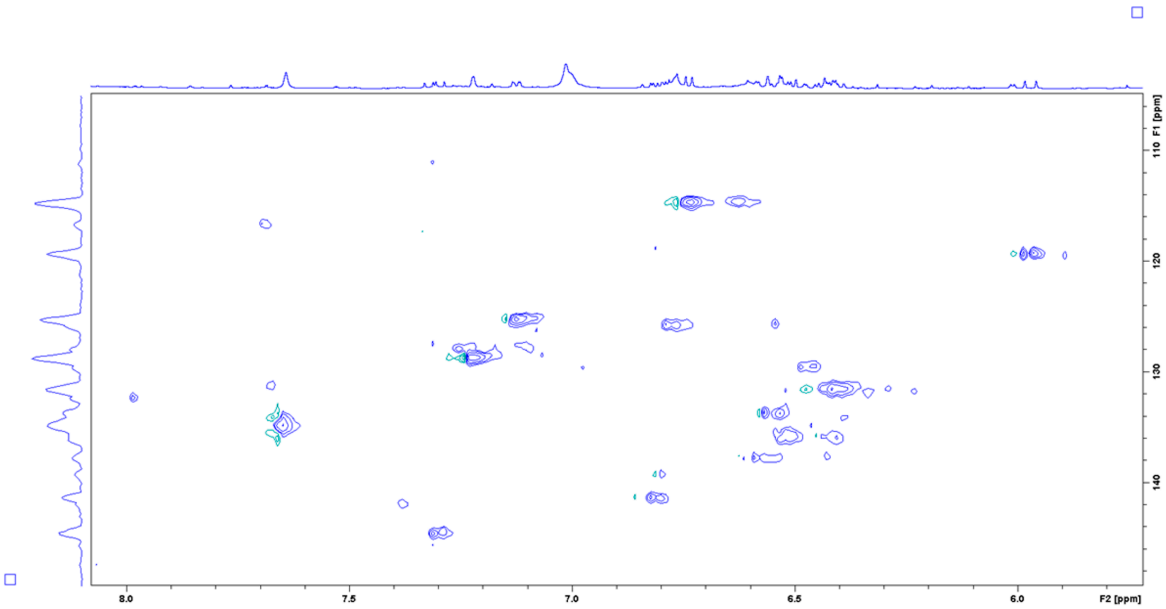

1005

1006 **Figure 2 – figure supplement 6**. HSQC spectrum of enriched aryl polyene in DMSO–δ_6 at 298

1007 K. Enhanced view of the aromatic region.

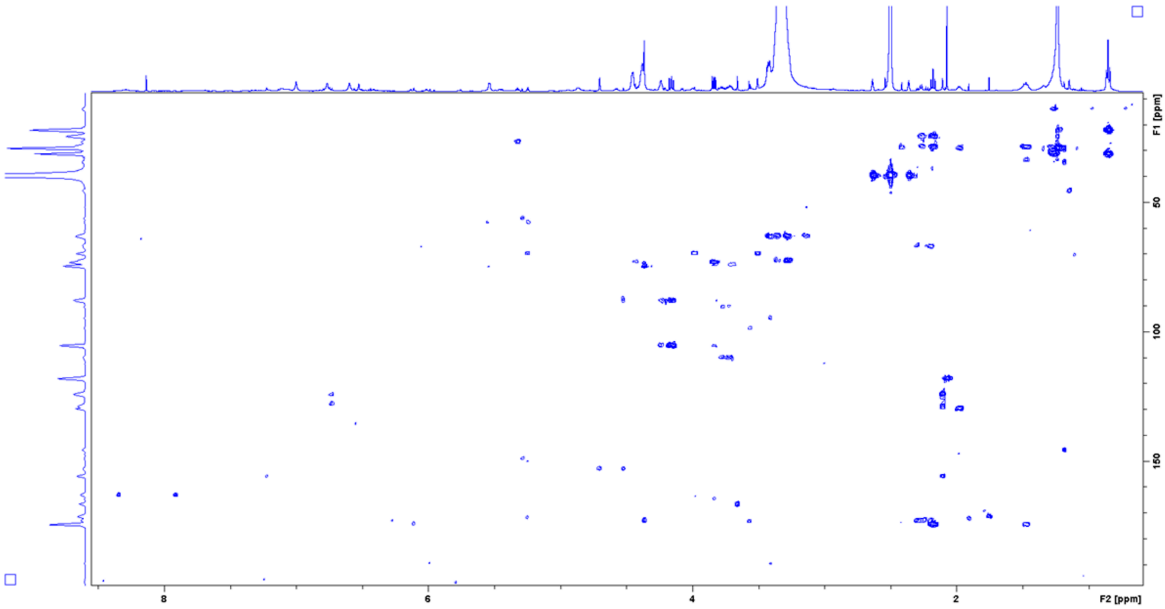

Figure 2 – figure supplement 7. COSY spectrum of enriched aryl polyene in DMSO–δ_6 at 298 K.

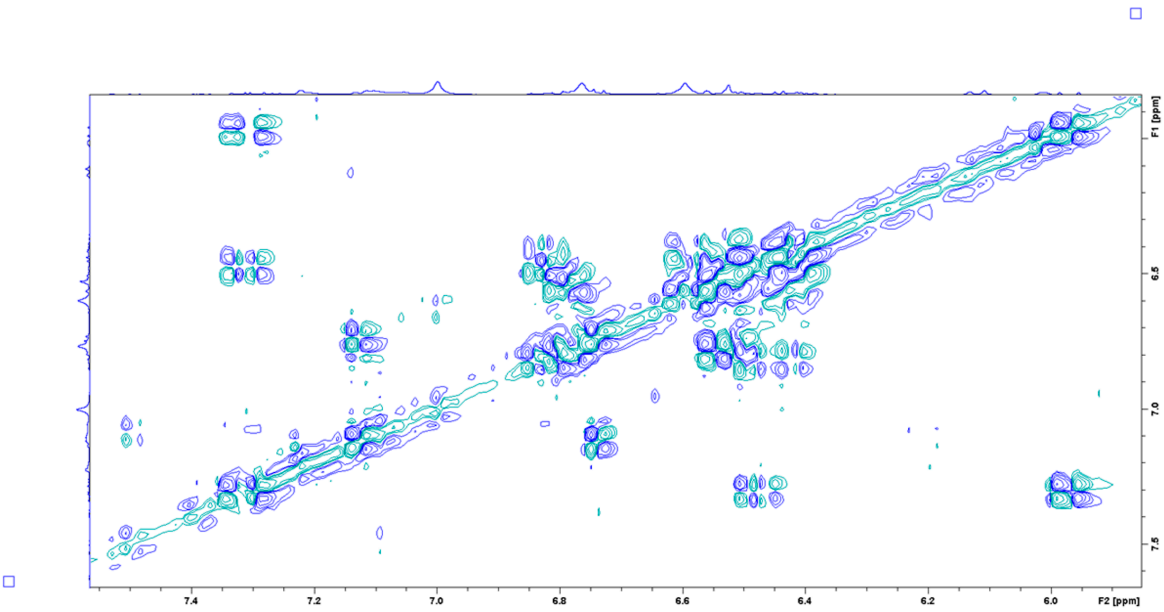

Figure 2 – figure supplement 8. COSY spectrum of enriched aryl polyene in DMSO–δ6 at 298 K. Enhanced view of the aromatic region.

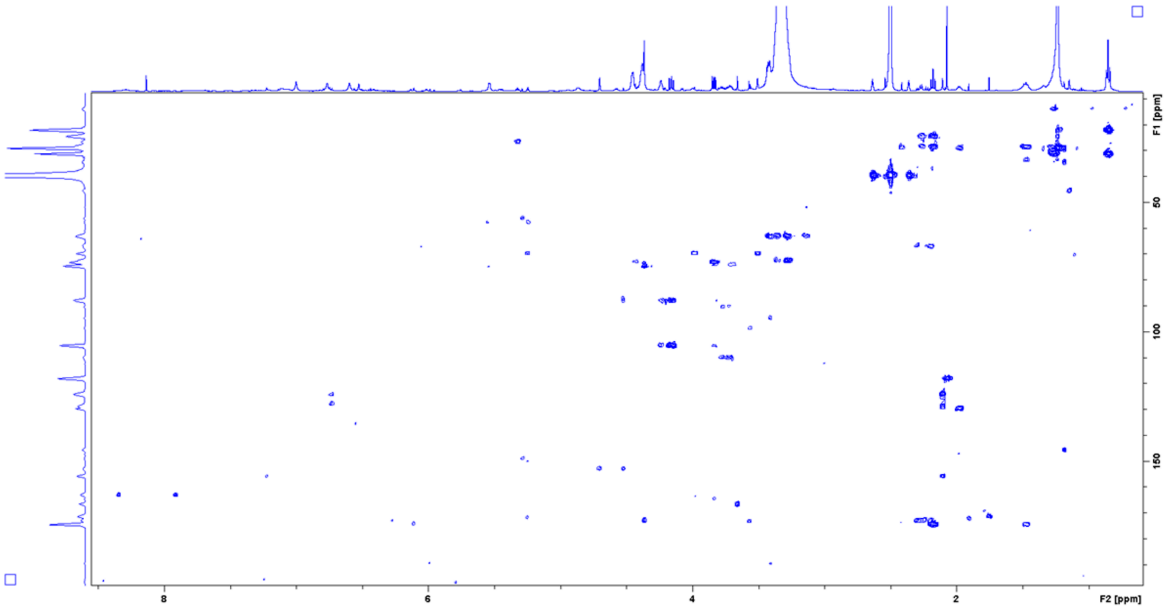

1015

1016 **Figure 2 – figure supplement 9.** HMBC spectrum of enriched aryl polyene in DMSO–δ6 at 298

1017

1018

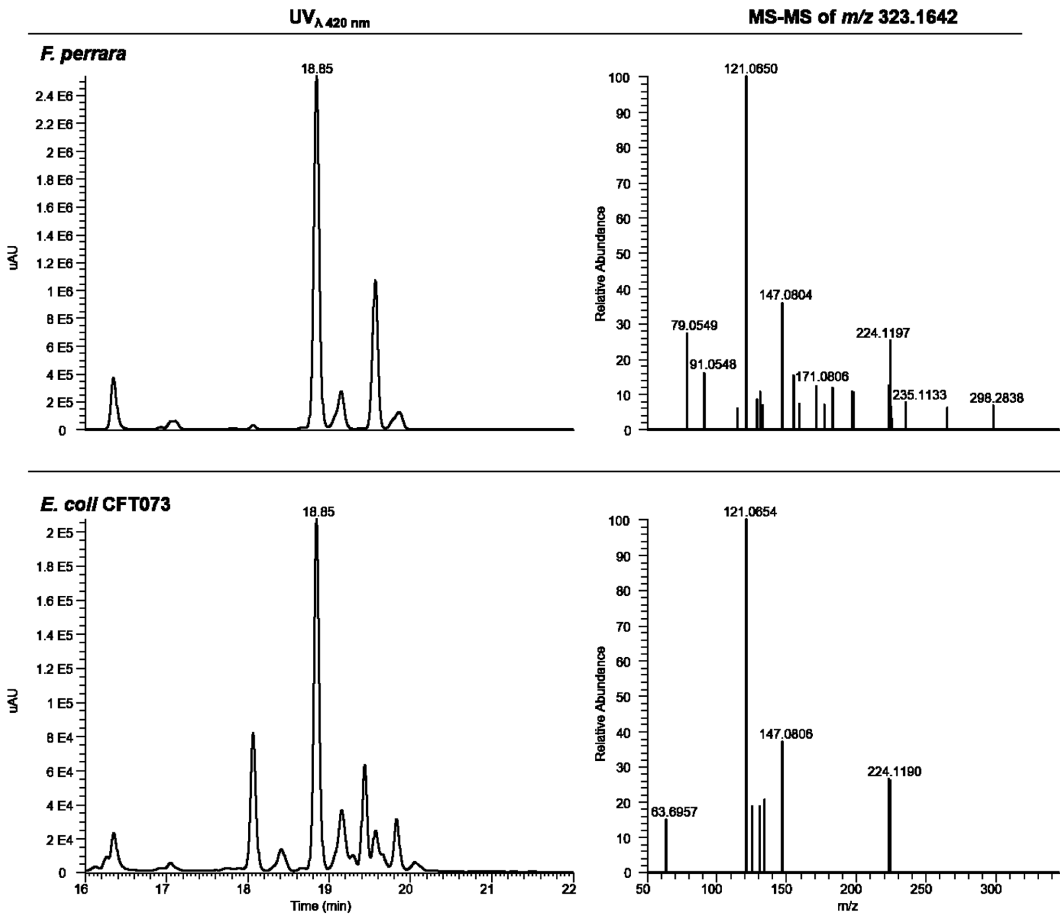

Figure 2 – figure supplement 10. HPLC-HRESIMS analysis of *F. perrara* and *E. coli* CFT073. At 18.85 min both extracts show strong absorbance at λ= 420 nm. The MS-MS fragmentation pattern of the ion *m/z* 323.1642 at that retention time shows a similar pattern in extracts from both strains.

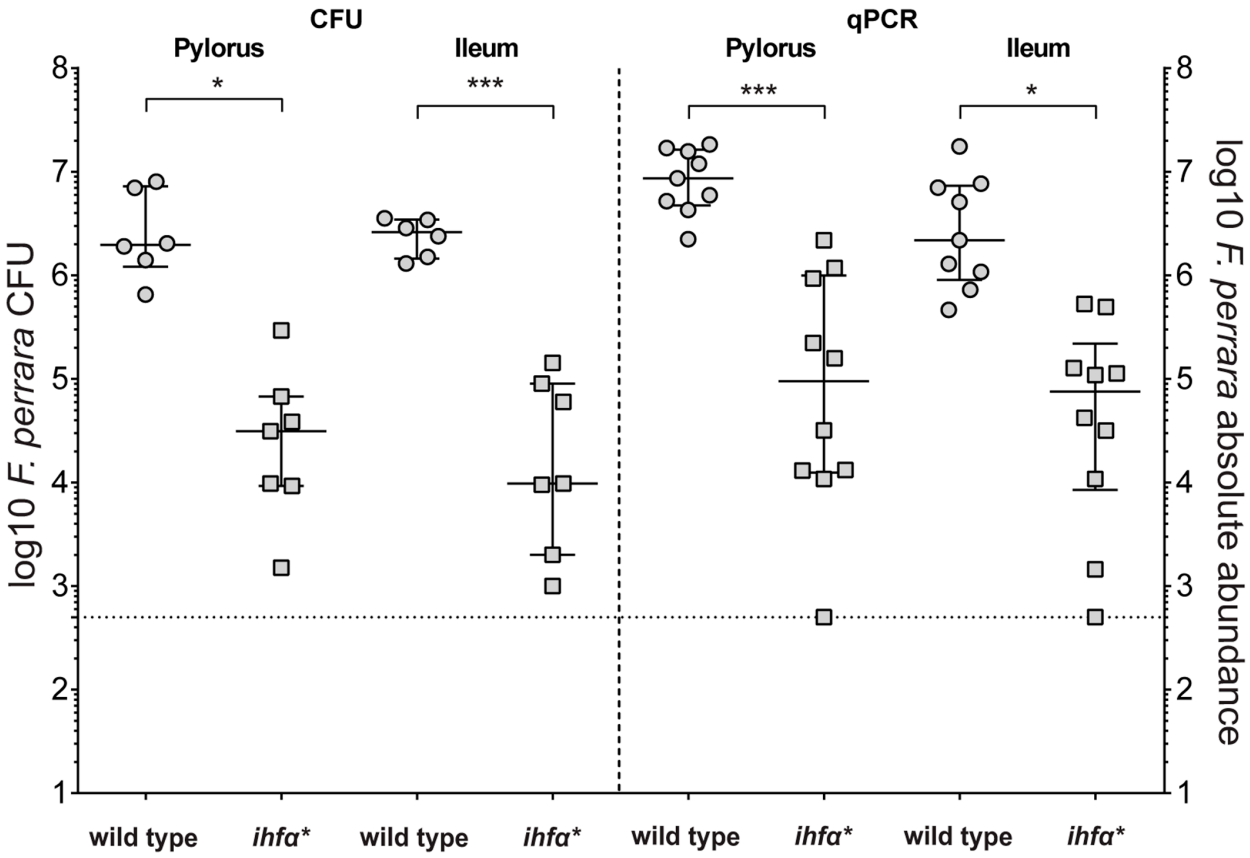

1024

1025 **Figure 3 – figure supplement 1. Quantification of *F. perrara* wt and *ihfA** in pylorus and**

1026 **ileum.** Mono-colonization of bees with *F. perrara* wt and *ihfA**. Colonization levels are measured

1027 by colony forming units (CFU) and quantitative PCR (qPCR) 10 days post colonization in the

1028 specified gut regions: pylorus and ileum. Wilcoxon rank-sum test was used to assess the

1029 statistical significance of differences. n=6.

1030

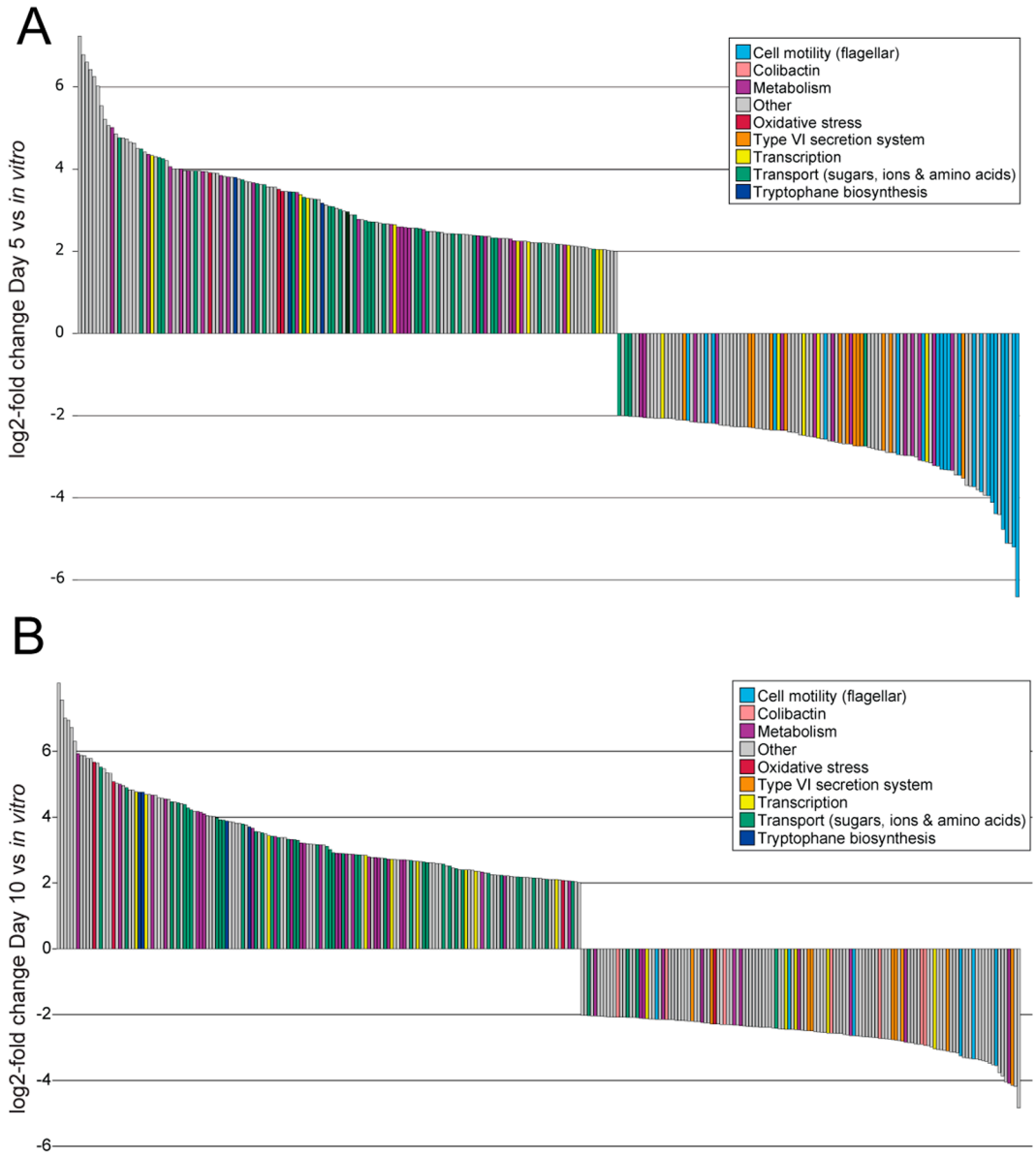

1031

1032 **Figure 5 – figure supplement 1. RNAseq comparison of *F. perrara* during *in vivo***
1033 **colonization compared to growth *in vitro*.** Significantly differentially expressed genes with a
1034 |log2-fold change| >|2| of *F. perrara* PEB0191 wt at day 5 (**A**) and day 10 (**B**) post colonization in
1035 comparison to growth *in vitro*. Genes are colored according to their category. The experiment was
1036 performed in quadruplicates, all genes displayed were significantly differentially expressed with
1037 $p<0.05$ and a FDR <0.05 (Exact test).

1038

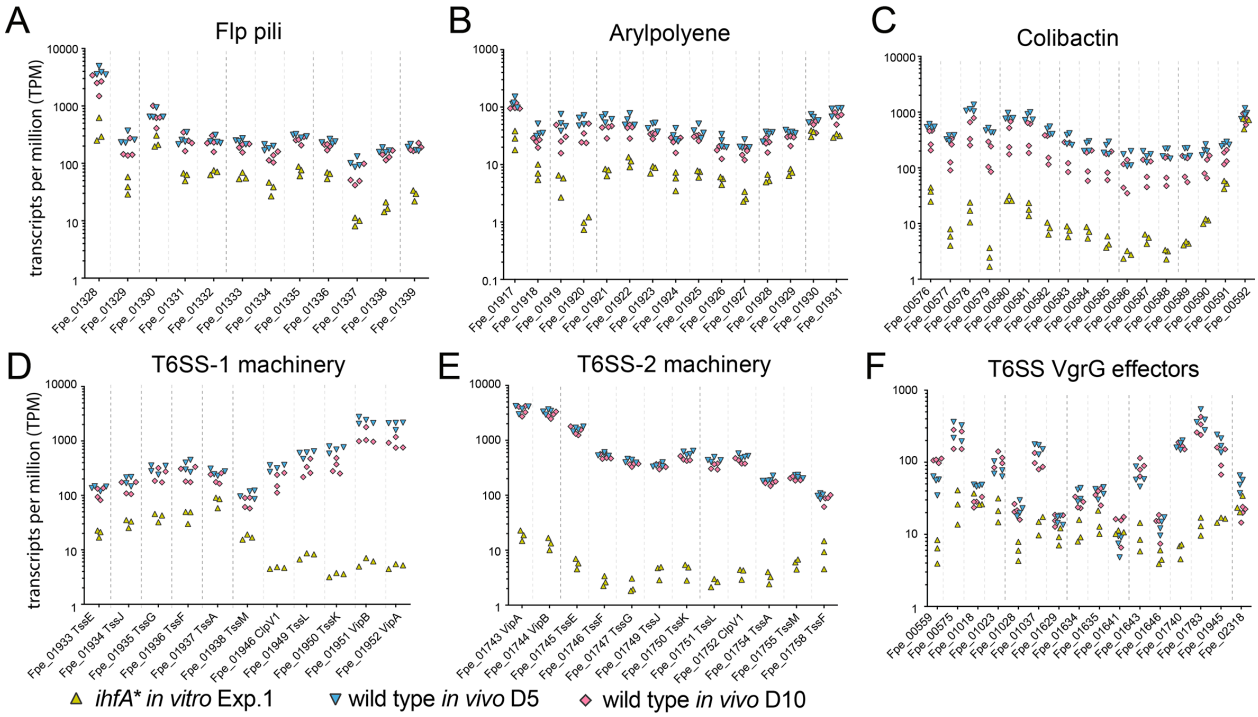

Figure 5 – figure supplement 2. **Gene expression of Ihf-regulated genes of *F. perrara* five days post-inoculation of gnotobiotic honey bees**. Same as Figure 5, but only time point Day 5 and Day 10 are depicted in comparison to *F. perrara ihfA* in vitro*.

1045

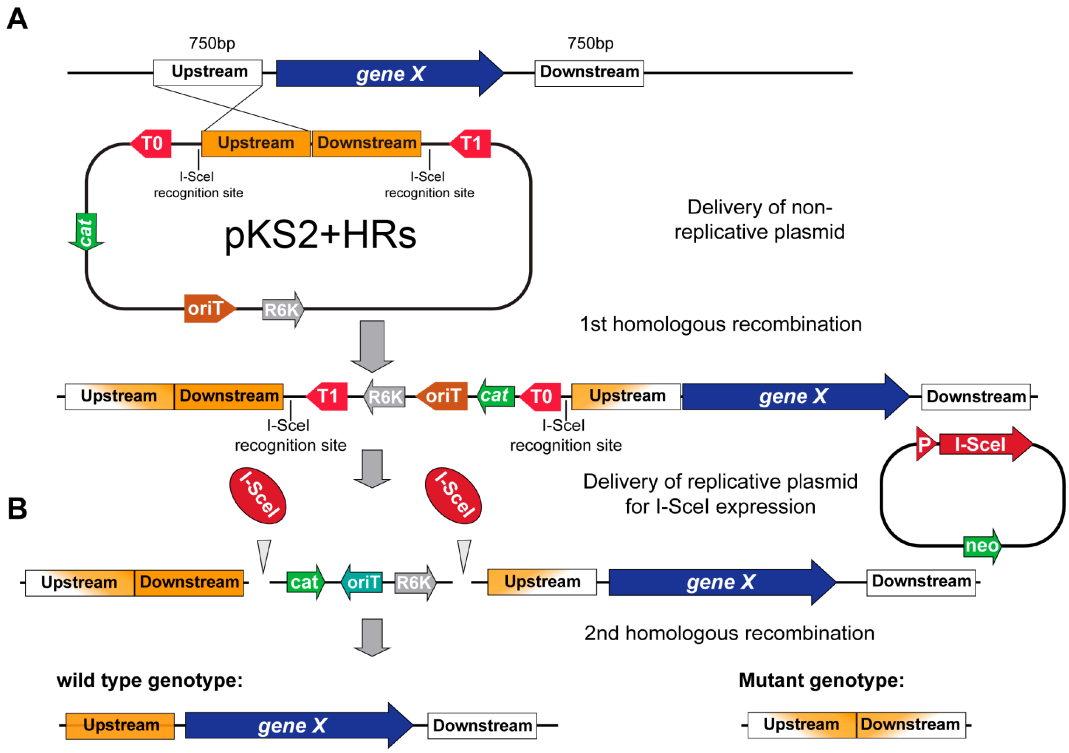

1046

1047 **Figure 6 – figure supplement 1. Scheme of the gene deletion strategy based on a two-step**
1048 **homologous recombination procedure.** (**A**) A non-replicative plasmid pKS2 integrates via
1049 homologous recombination of one of the two cloned 'homology regions' (HRs) upstream or
1050 downstream of the gene that is targeted for deletion. (**B**) In a second step, a replicative plasmid
1051 harboring the restriction enzyme I-SceI is transformed. I-SceI targets corresponding recognition
1052 sites located on pKS2 resulting in the selection of either revertant (wt genotypes) or mutant
1053 genotypes that underwent a second homologous recombination event in the region targeted for
1054 deletion. PCR screening and replica plating on different selective allows to identify to correct
1055 clones.

1056

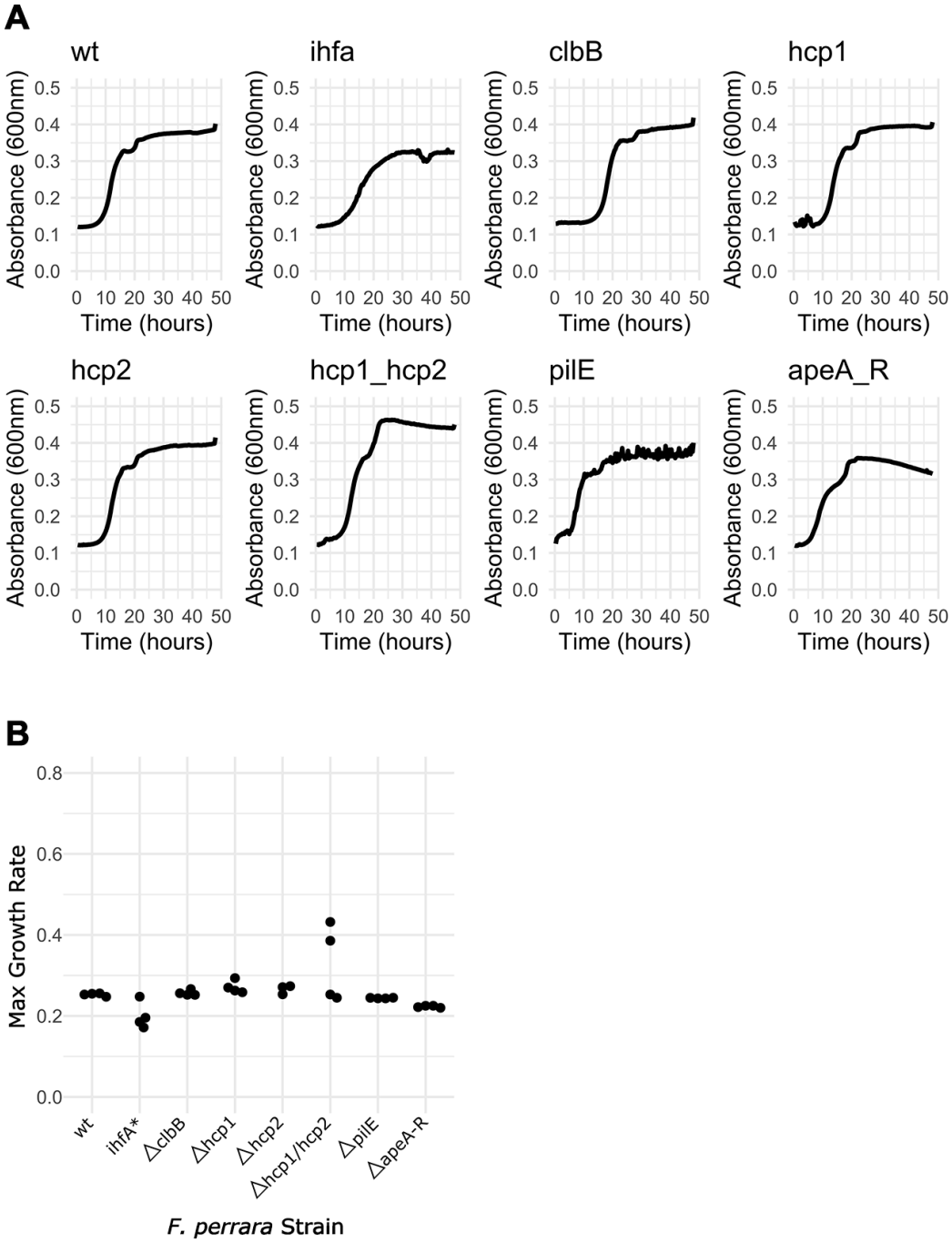

Figure 6 – figure supplement 2. Growth Curves for the different *Frischella* strains. (A) The six gene deletion mutants, *ihfa** and wt strains were diluted to OD_{600}=0.05 and grown in BHI under anaerobic conditions at 35ºC with continuous agitation. Absorbance was measured every 20 minutes for 48 hours. Per strain, four technical replicates were performed. **(B)** Max growth curve was calculated using the R package 'growthcurver'. For the *hcp2* mutant, only three technical replicates were considered due to a contamination in one of the technical replicates.

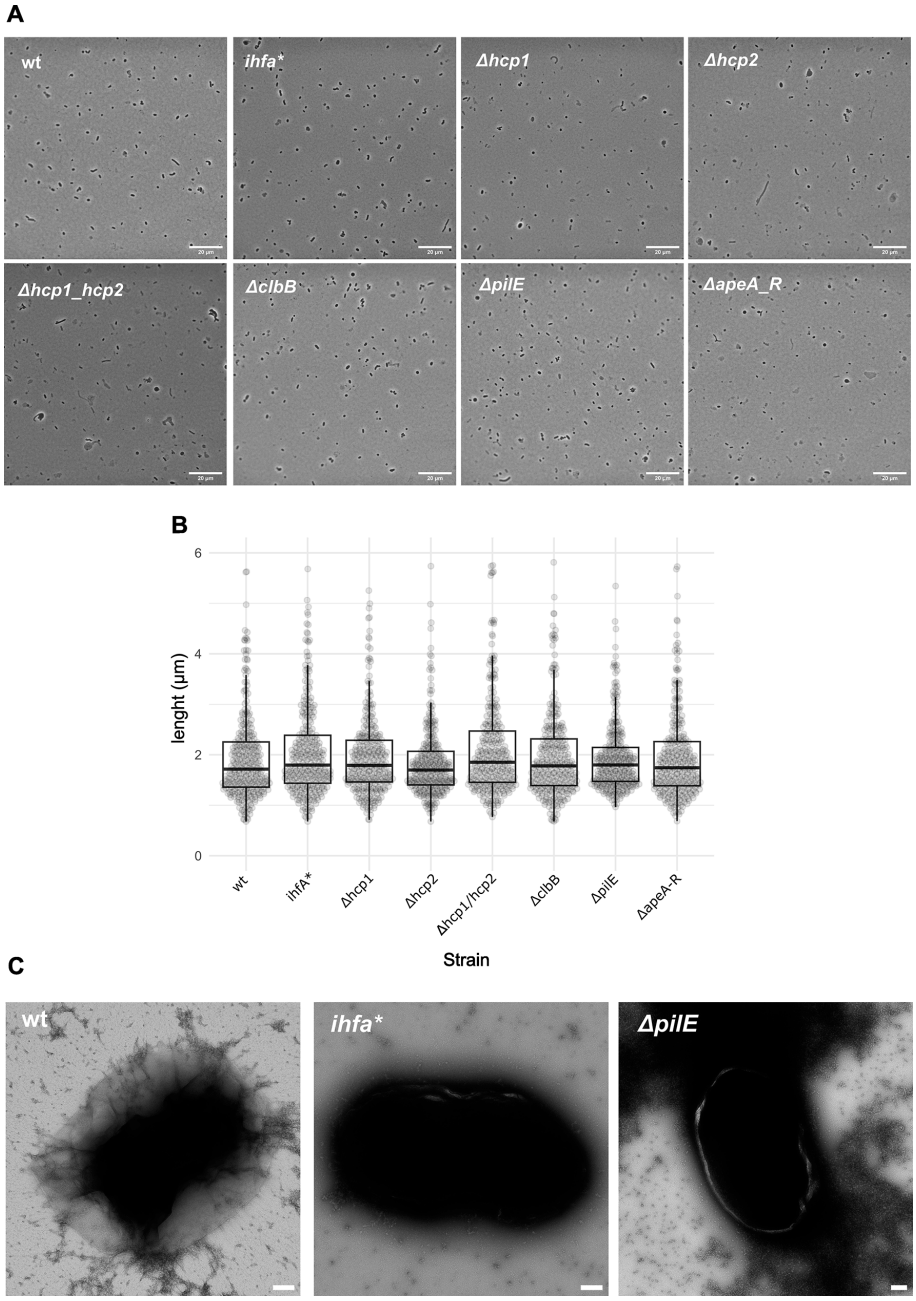

Figure 6 – figure supplement 3. Single Cell imaging of *F. perrara* strains. **(A)** The six gene deletion mutants, *ihfa**, and wt *F. perrara* strains were grown in liquid BHI, diluted to OD_{600}= 0.1, plated in agar patches and imaged using a Nikon Ti inverted light microscope. Images were taken with a 100x objective. Scale bar indicates 20µm. **(B)** Cell length was quantified using the MicrobeJ plugin of ImageJ. **(C)** Electron Microscopy images were obtained for the wt, *ihfA**, and *ΔpilE* strains. Scale bar indicates 200nm

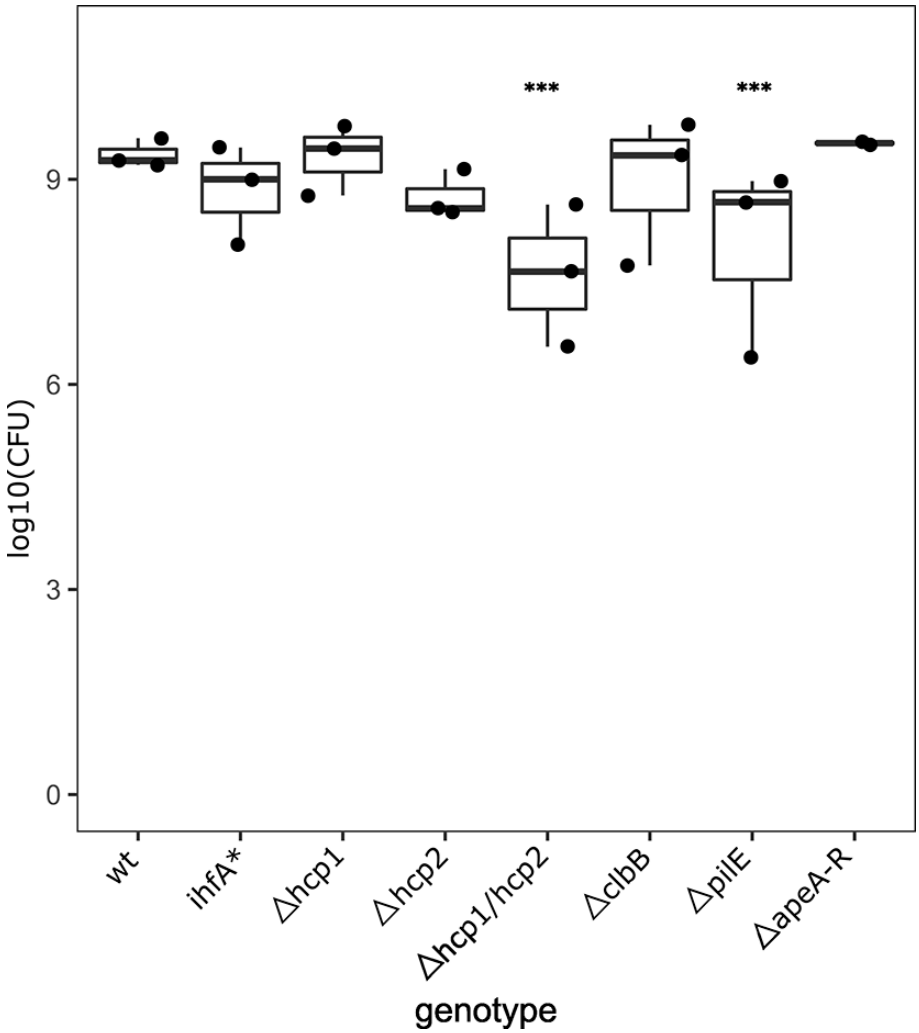

1074

1075 **Figure 6 – figure supplement 4. Correspondence between OD and CFU for *F. perrara***

1076 **genotypes.** For each *F. perrara* strain, a bacterial solution at OD_{600}=0.1 was prepared, serially

1077 diluted and plated in BHIA medium. The number of CFUs present in 5µl of solution at OD_{600}=0.1

1078 was calculated based on the counts obtained from the serial dilutions. Statistics were calculated

1079 using a linear model with negative binomial distribution: *** $p<0.0001$, ** $p<0.001$.

1080

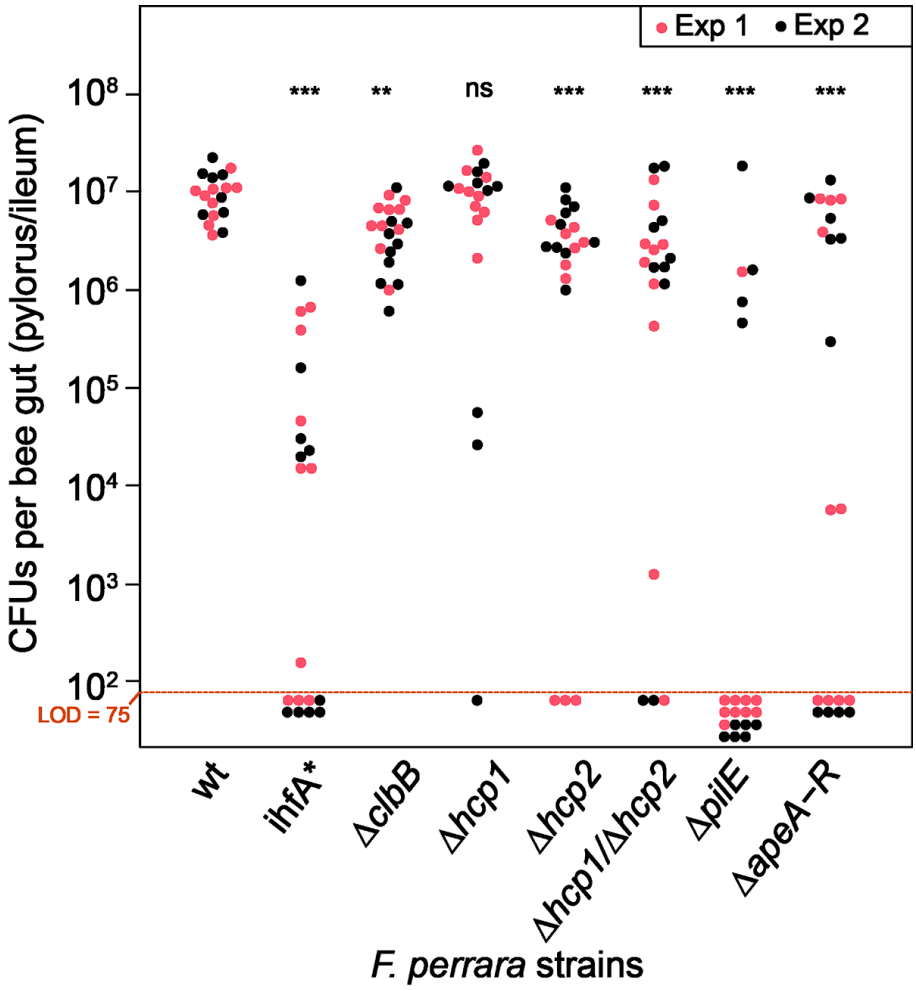

1081

1082 **Figure 6 – figure supplement 5**. Same graph as shown in **Figure 6** but data points are labelled
1083 by experiment.

1084

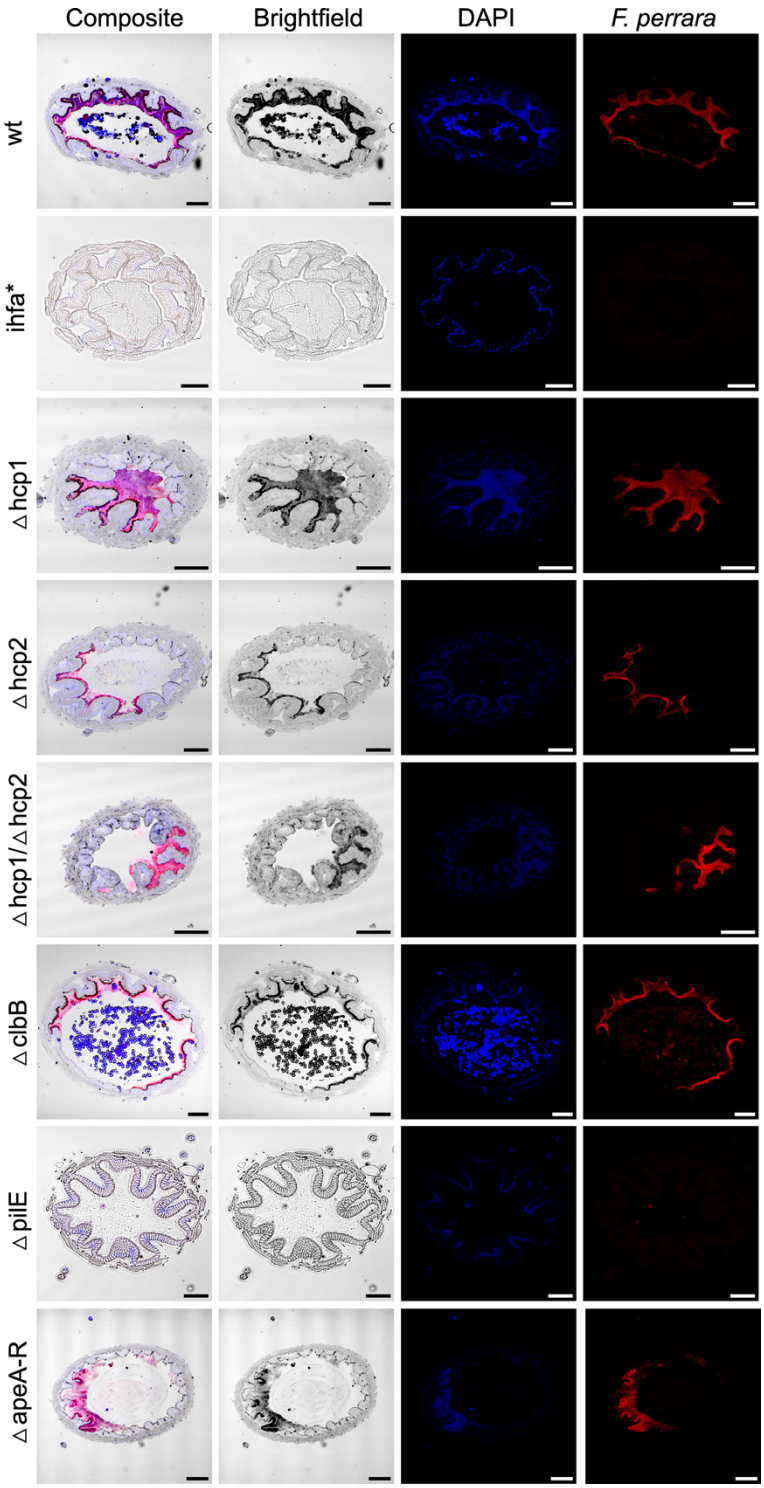

1085

1086 **Figure 6 – figure supplement 6. *F. perrara* colonization of the pylorus.** Composite images
1087 are the same as in **Figure 6**. These were obtained by merging the brightfield, DAPI, and *F.perrara*
1088 probe individual images. Images were obtained with the 5x objective of the Zeiss LSM900.
1089 Hybridizations were done with probes specific for *F. perrara* (magenta). DAPI counterstaining of
1090 host nuclei and bacteria is shown in blue.

1091

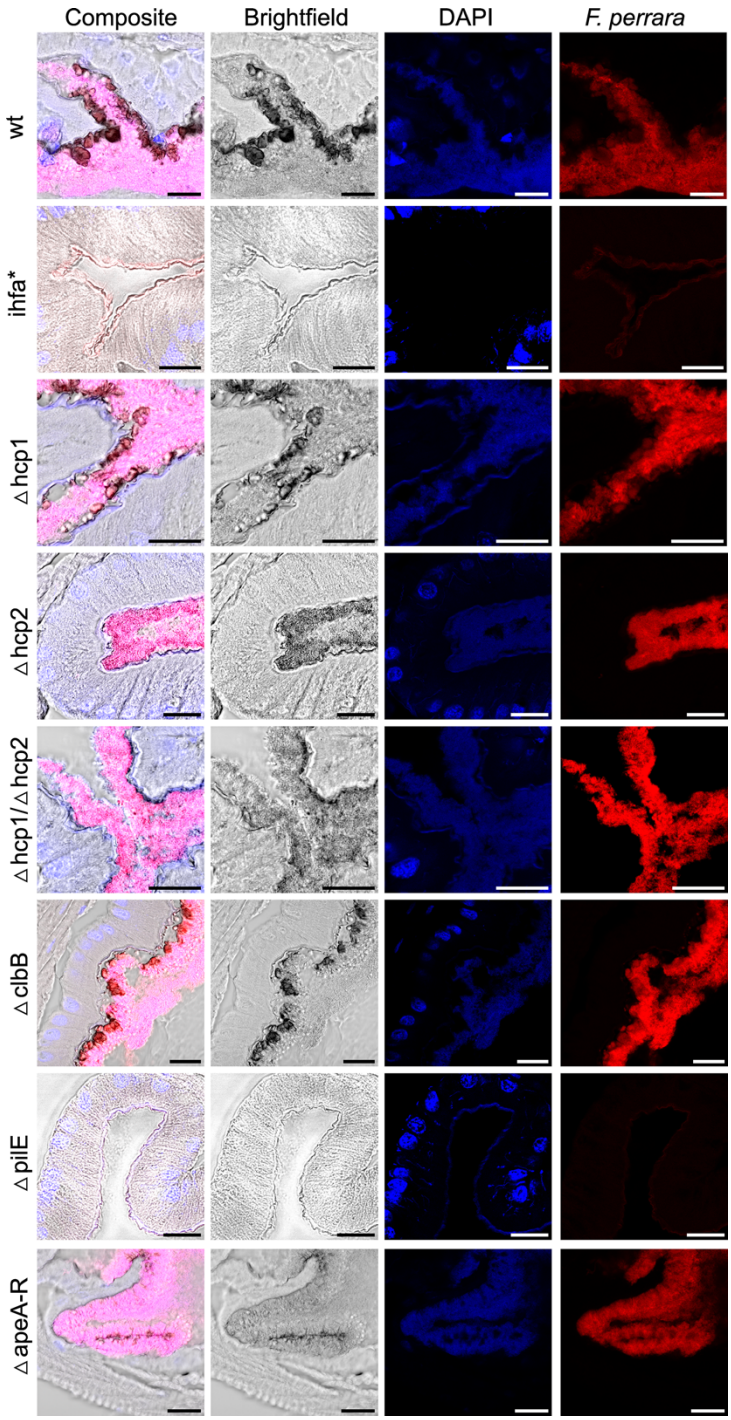

1092

1093 **Figure 6 – figure supplement 7**. ***F. perrara* colonization of the pylorus.** Composite images

1094 are the same as in **Figure 6**. These were obtained by merging the brightfield, DAPI and

1095 *F.perrara* probe images. Images were obtained with the 40x objective of the Zeiss LSM900.

1096 Hybridizations were done with probes specific for *F. perrara* (magenta). DAPI counterstaining of

1097 host nuclei and bacteria is shown in blue.

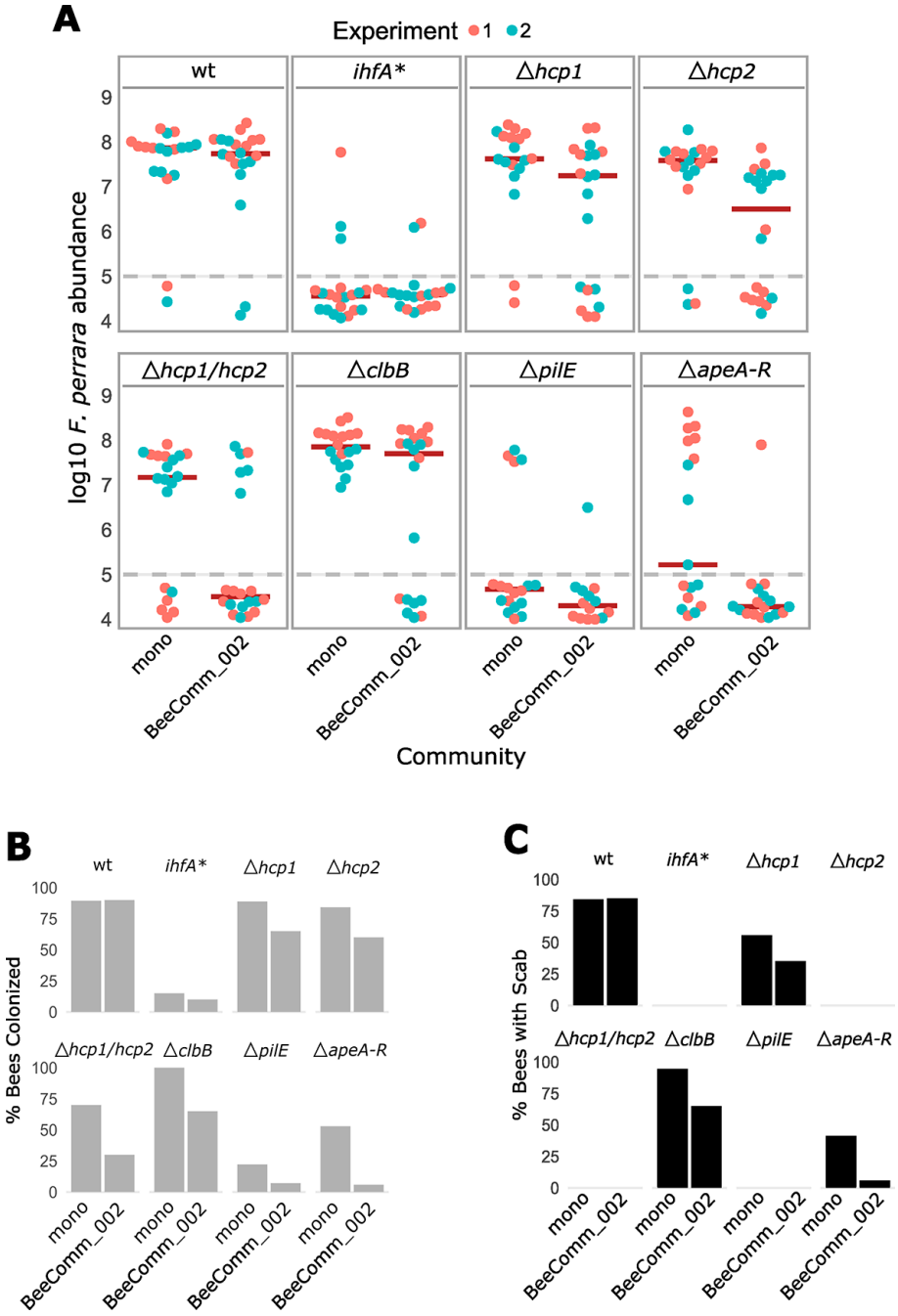

1098

1099 **Figure 7 – figure supplement 1**. **Colonization of wt, *ihfA** and gene-deletion mutants of *F.***

1100 ***perrara*. (A)** Same graph as shown in **Figure 7** but data points are labelled by experiment. **(B)**

1101 Percentage of bees that had colonization levels above the limit of detection. **(C)** Percentage of

1102 guts that had a scab.

Supplementary Tables

Supplementary Table 1. Chemical shifts of enriched aryl polyene in DMSO–δ6 at 298 K. Key COSY and HMBC correlation of the enriched polyene.

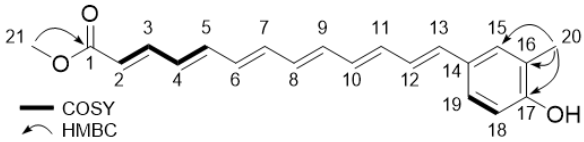

No	δ_C [ppm]	δ_H[ppm], mult.	coupling constant	integral
1	166.7			
2	119.3	5.97, d	*J*=15.1 Hz	0.5
3	144.6	7.33, dd	*J*=11.6 Hz *J*=15.1 Hz	1.2
4	129.5	6.47, dd overlap	*J*=11.6 Hz *J*=14.4 Hz	1.0
5	141.5	6.82, dd overlap	*J*= 11.4 Hz *J*= 14.5 Hz	0.9
6				
7				
8				
9				
10				
11				
12				
13				
14				
15	128.7	7.22, d	*J*=1.7 Hz	1.0
16	124.4			
17	155.9			
18	114.6	6.73, d	*J*=8.3 Hz	1.2
19	125.2	7.13, dd	*J*=1.9 Hz *J*=8.3 Hz	1.1
20	15.6	2.11, s		2.8
21	50.9	3.66, s overlap		3.5

Supplementary Table 2. Strains used in this study.

Species	Strain	Genotype*	Mutated gene	Reference	Parent strain
F. perrara	PEB0191/ ESL0157	wild type (wt)	None	(31)	Primary isolate
F. perrara	ESL0158	P83L (CCA→CTA) in *ihfA*	Fpe_00769	This study	PEB0191
F. perrara	ESL0910	P82L (CCA→CTA) in *ihfB;* Δ*apeO*	Fpe_00769; Fpe_01928	This study	PEB0191
F. perrara	ESL0922	L38S (TTA→TCA) in *ihfA;* Δ*pilE**	Fpe_00769; Fpe_00791*; Fpe_01328	This study	PEB0191
F. perrara	ESL0854	Δ*hcp1**	Fpe_01742	This study	PEB0191
F. perrara	ESL0855	Δ*hcp2*	Fpe_01947	This study	PEB0191
F. perrara	ESL0856	Δ*hcp1*, Δ*hcp2*	Fpe_01742, Fpe_01947	This study	PEB0191
F. perrara	ESL0888	Δ*clbB**	Fpe_00576	This study	PEB0191
F. perrara	ESL0921	Δ*pilE**	Fpe_01328	This study	PEB0191
F. perrara	ESL0957	Δ*apeA-R**	Fpe_01915-Fpe_01932	This study	PEB0191

1109 *re-sequencing of the genomes revealed that some of the strains (indicated with an asterisk)
1110 carried an additional point mutation. However, these mutations were located in random genes
1111 and included synonymous as well as non-synonymous base substitutions unlikely to have an
1112 effect on the observed phenotypes. The genomic analysis of the re-sequenced strains can be
1113 found on the Switchdrive: https://drive.switch.ch/index.php/s/kCNTp4g7n60ffMi.

1114

1115

1116 **Supplementary Table 3.** Primers used for qPCR quantification

Primer name	Target	Sequence 5' to 3'	Tm (°C)[a]	Amplicon size (bp)	# Gene loci per genome	Standard curve			
						Primer Efficiency, R^2	Slope, Intercept	LOD Cq[b] (#copies)	Reference
prPEN0013	Actin AB023025 *A. mellifera*	TGCCAACACTGTCCTTTCTG	58.4	156	-	1.896 = 89.6 %, 1.0	-3.6, 37.57	33.7 (10)	(83)
prPEN0014		AGAATTGACCCACCAATCCA	56.4						
prLK-Frisch-042-F	*F. perrara* 16S rRNA gene	GGAAGTTATGTGTGGGATAAGC	60.1	185	4	1.946 = 94.6 %, 0.995	-3.45, 38.04	31.7 (100)	(18)
prLK-Frisch-043-R		CTATTCTCAGGTTGAGCCCG	60.5						

1117 a - Melting temperatures were calculated with the online tool described in (Kibbe 2007)

1118 b - LOD refers to the limit of detection of primer sets, expressed here as the lowest number of

1119 plasmid copies reliably detected by qPCR when standard curves were performed

1120

1121

1122

Supplementary Table 4. Bacterial strains included in the defined community.

Bacterial species	Strain number
Snodgrassella alvi	ESL0145
Gilliamella apicola	ESL0309
Gilliamella apis	ESL0178
Gilliamella sp.	ESL0177
Bartonella apis	ESL0024
Bifidobacterium asteroides	ESL0197
Bifidobacterium asteroides	ESL0198
Lactobacillus Firm-5	ESL0185
Lactobacillus Firm-5	ESL0183
Lactobacillus Firm-5	ESL0184
Lactobacillus Firm-5	ESL0186
Lactobacillus Firm-4	ESL0294
Commensalibacter	ESL0284

1123

1124

1125

1126

References

1. M. Wu *et al.*, Genetic determinants of in vivo fitness and diet responsiveness in multiple human gut Bacteroides. *Science* **350**, aac5992 (2015).
2. S. M. Lee *et al.*, Bacterial colonization factors control specificity and stability of the gut microbiota. *Nature* **501**, 426-429 (2013).
3. G. E. Townsend *et al.*, Dietary sugar silences a colonization factor in a mammalian gut symbiont. *Proceedings of the National Academy of Sciences* **116**, 233-238 (2019).
4. G. E. Townsend *et al.*, A Master Regulator of Bacteroides thetaiotaomicron Gut Colonization Controls Carbohydrate Utilization and an Alternative Protein Synthesis Factor. *mBio* **11**, e03221-03219 (2020).
5. L. A. David *et al.*, Diet rapidly and reproducibly alters the human gut microbiome. *Nature* **505**, 559-563 (2014).
6. A. Nakajima *et al.*, IgA regulates the composition and metabolic function of gut microbiota by promoting symbiosis between bacteria. *Journal of Experimental Medicine* **215**, 2019-2034 (2018).
7. J. E. Powell, S. P. Leonard, W. K. Kwong, P. Engel, N. A. Moran, Genome-wide screen identifies host colonization determinants in a bacterial gut symbiont. *Proceedings of the National Academy of Sciences of the United States of America* 10.1073/pnas.1610856113 (2016).
8. T. Ohbayashi *et al.*, Insect's intestinal organ for symbiont sorting. *Proceedings of the National Academy of Sciences* **112**, E5179-E5188 (2015).
9. H. Salem *et al.*, Drastic Genome Reduction in an Herbivore’s Pectinolytic Symbiont. *Cell* **171**, 1520-1531.e1513 (2017).
10. Y. Kikuchi, T. Ohbayashi, S. Jang, P. Mergaert, Burkholderia insecticola triggers midgut closure in the bean bug Riptortus pedestris to prevent secondary bacterial infections of midgut crypts. *The ISME journal* 10.1038/s41396-020-0633-3 (2020).

11. W. K. Kwong, N. A. Moran, Gut microbial communities of social bees. *Nature reviews. Microbiology* **14**, 374-384 (2016).

12. G. Bonilla-Rosso, P. Engel, Functional roles and metabolic niches in the honey bee gut microbiota. *Curr Opin Microbiol* **43**, 69-76 (2018).

13. W. K. Kwong *et al.*, Dynamic microbiome evolution in social bees. *Sci Adv* **3**, e1600513 (2017).

14. P. Engel, K. D. Bartlett, N. A. Moran, The Bacterium Frischella perrara Causes Scab Formation in the Gut of its Honeybee Host. *mBio* **6** (2015).

15. V. G. Martinson *et al.*, A simple and distinctive microbiota associated with honey bees and bumble bees. *Molecular ecology* **20**, 619-628 (2011).

16. J. E. Powell, V. G. Martinson, K. Urban-Mead, N. A. Moran, Routes of Acquisition of the Gut Microbiota of the Honey Bee Apis mellifera. *Appl Environ Microbiol* **80**, 7378-7387 (2014).

17. O. Emery, K. Schmidt, P. Engel, Immune system stimulation by the gut symbiont Frischella perrara in the honey bee (Apis mellifera). *Molecular ecology* **26**, 2576-2590 (2017).

18. L. Kesnerova *et al.*, Disentangling metabolic functions of bacteria in the honey bee gut. *bioRxiv* 10.1101/157461 (2017).

19. K. Raymann, L. M. Bobay, N. A. Moran, Antibiotics reduce genetic diversity of core species in the honeybee gut microbiome. *Mol Ecol* **27**, 2057-2066 (2018).

20. H. Zheng, J. E. Powell, M. I. Steele, C. Dietrich, N. A. Moran, Honeybee gut microbiota promotes host weight gain via bacterial metabolism and hormonal signaling. *Proceedings of the National Academy of Sciences of the United States of America* **114**, 4775-4780 (2017).

21. S. Brochet *et al.*, Niche partitioning facilitates coexistence of closely related honey bee gut bacteria. *Elife* **10** (2021).

22. K. M. Ellegaard *et al.*, Genomic changes underlying host specialization in the bee gut symbiont Lactobacillus Firm5. *Molecular ecology* **28**, 2224-2237 (2019).

23. K. M. Ellegaard, P. Engel, Genomic diversity landscape of the honey bee gut microbiota. *Nature communications* **10**, 446 (2019).

24. P. Engel, V. G. Martinson, N. A. Moran, Functional diversity within the simple gut microbiota of the honey bee. *Proceedings of the National Academy of Sciences of the United States of America* **109**, 11002-11007 (2012).

25. W. K. Kwong, P. Engel, H. Koch, N. A. Moran, Genomics and host specialization of honey bee and bumble bee gut symbionts. *Proceedings of the National Academy of Sciences of the United States of America* **111**, 11509-11514 (2014).

26. W. K. Kwong *et al.*, Dynamic microbiome evolution in social bees. *Science Advances* **3** (2017).

27. J. Ludvigsen, D. Porcellato, G. V. Amdam, K. Rudi, Addressing the diversity of the honeybee gut symbiont Gilliamella: description of Gilliamella apis sp. nov., isolated from the gut of honeybees (Apis mellifera). *Int J Syst Evol Microbiol* **68**, 1762-1770 (2018).

28. M. I. Steele, W. K. Kwong, M. Whiteley, N. A. Moran, Diversification of Type VI Secretion System Toxins Reveals Ancient Antagonism among Bee Gut Microbes. *mBio* **8** (2017).

29. H. Zheng *et al.*, Division of labor in honey bee gut microbiota for plant polysaccharide digestion. *Proceedings of the National Academy of Sciences* **116**, 25909-25916 (2019).

30. M. Volkmann *et al.*, Orbus hercynius gen. nov., sp. nov., isolated from faeces of wild boar, is most closely related to members of the orders 'Enterobacteriales' and Pasteurellales. *Int J Syst Evol Microbiol* **60**, 2601-2605 (2010).

31. P. Engel, W. K. Kwong, N. A. Moran, Frischella perrara gen. nov., sp. nov., a gammaproteobacterium isolated from the gut of the honeybee, Apis mellifera. *International Journal of Systematic and Evolutionary Microbiology* **63**, 3646-3651 (2013).

32. V. G. Martinson, J. Moy, N. A. Moran, Establishment of characteristic gut bacteria during development of the honeybee worker. *Appl Environ Microbiol* **78**, 2830-2840 (2012).

33. S. P. Leonard *et al.*, Genetic Engineering of Bee Gut Microbiome Bacteria with a Toolkit for Modular Assembly of Broad-Host-Range Plasmids. *ACS Synth Biol* **7**, 1279-1290 (2018).

34. P. Engel, K. D. Bartlett, N. A. Moran, The Bacterium Frischella perrara Causes Scab Formation in the Gut of its Honeybee Host. *MBio* **6**, e00193-00115 (2015).

35. L. Kesnerova *et al.*, Gut microbiota structure differs between honeybees in winter and summer. *ISME J* **14**, 801-814 (2020).

36. L. A. Wolter, S. Suenami, R. Miyazaki, Frischella japonica sp. nov., an anaerobic member of the Orbales in the Gammaproteobacteria, isolated from the gut of the eastern honey bee, Apis cerana japonica Fabricius. *Int J Syst Evol Microbiol* **71** (2019).

37. P. Engel, M. I. Vizcaino, J. M. Crawford, Gut symbionts from distinct hosts exhibit genotoxic activity via divergent colibactin biosynthesis pathways. *Appl Environ Microbiol* **81**, 1502-1512 (2015).

38. P. Engel, W. K. Kwong, N. A. Moran, Frischella perrara gen. nov., sp. nov., a gammaproteobacterium isolated from the gut of the honeybee, Apis mellifera. *Int J Syst Evol Microbiol* **63**, 3646-3651 (2013).

39. D. I. Friedman, Integration host factor: A protein for all reasons. *Cell* **55**, 545-554 (1988).

40. M. Freundlich, N. Ramani, E. Mathew, A. Sirko, P. Tsui, The role of integration host factor in gene expression in Escherichia coli. *Molecular microbiology* **6**, 2557-2563 (1992).

41. N. Goosen, P. van de Putte, The regulation of transcription initiation by integration host factor. *Molecular microbiology* **16**, 1-7 (1995).

42. P. A. Rice, S.-w. Yang, K. Mizuuchi, H. A. Nash, Crystal Structure of an IHF-DNA Complex: A Protein-Induced DNA U-Turn. *Cell* **87**, 1295-1306 (1996).

43. P. Cimermancic *et al.*, Insights into secondary metabolism from a global analysis of prokaryotic biosynthetic gene clusters. *Cell* **158**, 412-421 (2014).

44. A. K. Goel, L. Rajagopal, N. Nagesh, R. V. Sonti, Genetic Locus Encoding Functions Involved in Biosynthesis and Outer Membrane Localization of Xanthomonadin in Xanthomonas oryzae pv. oryzae. *J Bacteriol* **184**, 3539-3548 (2002).

45. A. R. Poplawsky, S. C. Urban, W. Chun, Biological role of xanthomonadin pigments in Xanthomonas campestris pv. campestris. *Appl Environ Microbiol* **66**, 5123-5127 (2000).

46. T. A. Schoner *et al.*, Aryl Polyenes, a Highly Abundant Class of Bacterial Natural Products, Are Functionally Related to Antioxidative Carotenoids. *Chembiochem* **17**, 247-253 (2016).

47. L. J. Lee, J. A. Barrett, R. K. Poole, Genome-wide transcriptional response of chemostat-cultured Escherichia coli to zinc. *J Bacteriol* **187**, 1124-1134 (2005).

48. K. Hantke, Iron and metal regulation in bacteria. *Current opinion in microbiology* **4**, 172-177 (2001).

49. M. Basler, B. T. Ho, J. J. Mekalanos, Tit-for-tat: type VI secretion system counterattack during bacterial cell-cell interactions. *Cell* **152**, 884-894 (2013).

50. R. Gallegos-Monterrosa, S. J. Coulthurst, The ecological impact of a bacterial weapon: microbial interactions and the Type VI secretion system. *FEMS Microbiol Rev* **45** (2021).

51. L. Zulianello, P. van Ulsen, P. van de Putte, N. Goosen, Participation of the Flank Regions of the Integration Host Factor Protein in the Specificity and Stability of DNA Binding. *Journal of Biological Chemistry* **270**, 17902-17907 (1995).

52. J. A. Jurcisek, K. L. Brockman, L. A. Novotny, S. D. Goodman, L. O. Bakaletz, Nontypeable Haemophilus influenzae releases DNA and DNABII proteins via a T4SS-like complex and ComE of the type IV pilus machinery. *Proc Natl Acad Sci U S A* **114**, E6632-E6641 (2017).

53. A. S. Utada *et al.*, Vibrio cholerae use pili and flagella synergistically to effect motility switching and conditional surface attachment. *Nat Commun* **5**, 4913 (2014).

54. M. Tomich, P. J. Planet, D. H. Figurski, The tad locus: postcards from the widespread colonization island. *Nature reviews. Microbiology* **5**, 363-375 (2007).

55. A. Shime-Hattori *et al.*, Two type IV pili of Vibrio parahaemolyticus play different roles in biofilm formation. *FEMS Microbiol Lett* **264**, 89-97 (2006).

56. L. Craig, M. E. Pique, J. A. Tainer, Type IV pilus structure and bacterial pathogenicity. *Nature reviews. Microbiology* **2**, 363-378 (2004).

57. I. Johnston *et al.*, Identification of essential genes for Escherichia coli aryl polyene biosynthesis and function in biofilm formation. *NPJ Biofilms Microbiomes* **7**, 56 (2021).

58. T. Kuraishi, A. Hori, S. Kurata, Host-microbe interactions in the gut of Drosophila melanogaster. *Front Physiol* **4**, 375 (2013).

59. E. M. Ha, C. T. Oh, Y. S. Bae, W. J. Lee, A direct role for dual oxidase in Drosophila gut immunity. *Science* **310**, 847-850 (2005).

60. J. P. Nougayrede *et al.*, Escherichia coli induces DNA double-strand breaks in eukaryotic cells. *Science* **313**, 848-851 (2006).

61. G. Cuevas-Ramos *et al.*, Escherichia coli induces DNA damage in vivo and triggers genomic instability in mammalian cells. *Proc Natl Acad Sci U S A* **107**, 11537-11542 (2010).

62. J. C. Arthur *et al.*, Intestinal inflammation targets cancer-inducing activity of the microbiota. *Science* **338**, 120-123 (2012).

63. J. D. Mougous *et al.*, A virulence locus of Pseudomonas aeruginosa encodes a protein secretion apparatus. *Science* **312**, 1526-1530 (2006).

64. M. J. Coyne, L. E. Comstock, Type VI Secretion Systems and the Gut Microbiota. *Microbiol Spectr* **7** (2019).

65. S. Coulthurst, The Type VI secretion system: a versatile bacterial weapon. *Microbiology (Reading)* **165**, 503-515 (2019).

66. J. Monjaras Feria, M. A. Valvano, An Overview of Anti-Eukaryotic T6SS Effectors. *Front Cell Infect Microbiol* **10**, 584751 (2020).

67. M. I. Steele, N. A. Moran, Evolution of Interbacterial Antagonism in Bee Gut Microbiota Reflects Host and Symbiont Diversification. *mSystems* **6** (2021).

68. E. Powell, N. Ratnayeke, N. A. Moran, Strain diversity and host specificity in a specialized gut symbiont of honeybees and bumblebees. *Mol Ecol* **25**, 4461-4471 (2016).

69. J. Pan *et al.*, Integration Host Factor Modulates the Expression and Function of T6SS2 in Vibrio fluvialis. *Frontiers in microbiology* **9** (2018).

70. X. Chen, C. Yu, S. Li, X. Li, Q. Liu, Integration Host Factor Is Essential for Biofilm Formation, Extracellular Enzyme, Zeamine Production, and Virulence in Dickeya zeae. *Molecular Plant-Microbe Interactions®* **32**, 325-335 (2018).

71. O. Nikolayeva, M. D. Robinson, edgeR for differential RNA-seq and ChIP-seq analysis: an application to stem cell biology. *Methods Mol Biol* **1150**, 45-79 (2014).

72. M. D. Robinson, A. Oshlack, A scaling normalization method for differential expression analysis of RNA-seq data. *Genome Biology* **11**, R25 (2010).

73. G. P. Wagner, K. Kin, V. J. Lynch, Measurement of mRNA abundance using RNA-seq data: RPKM measure is inconsistent among samples. *Theory Biosci Theor Den Biowissenschaften* **131** (2012).

74. N. H. Freese, D. C. Norris, A. E. Loraine, Integrated genome browser: visual analytics platform for genomics. *Bioinformatics* **32**, 2089-2095 (2016).

75. L. Kesnerova *et al.*, Gut microbiota structure differs between honeybees in winter and summer. *The ISME journal* 10.1038/s41396-019-0568-8 (2019).

76. C. A. Schneider, W. S. Rasband, K. W. Eliceiri, NIH Image to ImageJ: 25 years of image analysis. *Nat Methods* **9**, 671-675 (2012).

77. A. Ducret, E. M. Quardokus, Y. V. Brun, MicrobeJ, a tool for high throughput bacterial cell detection and quantitative analysis. *Nat Microbiol* **1**, 16077 (2016).

78. E. Martinez-Garcia *et al.*, SEVA 3.0: an update of the Standard European Vector Architecture for enabling portability of genetic constructs among diverse bacterial hosts. *Nucleic acids research* **48**, 3395 (2020).

79. A. Harms *et al.*, A bacterial toxin-antitoxin module is the origin of inter-bacterial and inter-kingdom effectors of Bartonella. *PLoS Genet* **13**, e1007077 (2017).

80. D. E. Deatherage, J. E. Barrick, Identification of mutations in laboratory-evolved microbes from next-generation sequencing data using breseq. *Methods Mol Biol* **1151**, 165-188 (2014).

81. C. M. Elso *et al.*, Leishmaniasis host response loci (lmr1-3) modify disease severity through a Th1/Th2-independent pathway. *Genes Immun* **5**, 93-100 (2004).

82. L. Guy, J. R. Kultima, S. G. Andersson, genoPlotR: comparative gene and genome visualization in R. *Bioinformatics* **26**, 2334-2335 (2010).

83. M. S. Zufelato, A. P. Lourenço, Z. L. Simões, J. A. Jorge, M. M. Bitondi, Phenoloxidase activity in Apis mellifera honey bee pupae, and ecdysteroid-dependent expression of the prophenoloxidase mRNA. *Insect biochemistry and molecular biology* **34**, 1257-1268 (2004).